Pertanika Journal of Science & Technology

Volume 14 Nos. 1 & 2, 2006

Contents

Pertanika J. Sci. & Technol. **14(1 & 2)**: 1 - 11 (2006)
ISSN: 0128-7680

A Study of Dopant Composition and Sintering Time Effect on Thermal Diffusivity of Doped and Undoped BSCCO Superconducting Ceramics

Josephine L.Y.C, W. Mahmood Mat Yunus, Zaidan Abd. Wahab, Imad Hamadneh & Abdul Halim Shaari

Department of Physics, Faculty of Science and Environmental Studies, Universiti Putra Malaysia,43400 UPM, Serdang, Selangor, Malaysia

Received: 8 April 2003

ABSTRAK

Dalam kertas ini, sampel superkonduktor BSCCO yang didop dan yang tidak didop disediakan pada pelbagai suhu sinteran (cth. 24, 48 dan 100 jam) telah dikaji sifat resapan termanya. Nilai resapan terma telah diukur pada suhu bilik menggunakan teknik sinar kilat. Punca pengujaan dan sistem pengesanan merangkumi satu lampu kilat kamera dan termogandingan jenis K. Nilai resapan terma yang diukur didapati sangat bergantung pada kepekatan dopan, tetapi sebaliknya bebas daripada faktor masa sinteran. Dalam kajian ini, morfologi permukaan diperhati menggunakan imbasan mikroskopi elektron (SEM) adalah menyokong kuat hasil resapan terma yang diperoleh.

ABSTRACT

In this paper, the undoped and Sm doped BSCCO superconducting ceramic samples prepared at various sintering times (i.e. 24, 48 and 100 hours) were investigated for their thermal diffusivity. The thermal diffusivity value was measured at room temperature using photoflash technique. The excitation source and detection system consisted of a high intensity camera flash and K–type thermocouple. The measured thermal diffusivity value was found to be highly dependent on dopant concentration but not on sintering time. In this study, the surface morphology observed using Scanning Electron Microscopy (SEM) strongly supports the thermal diffusivity results.

Keywords: Dopant composition, thermal diffusivity, BCSSO, sintering time

INTRODUCTION

Bi(Pb)–Sr–Ca–Cu–O System has been investigated by many research groups concerning the preparation, superconducting properties, effect of doping as well as the structure of these compounds (Trong *et al.* 1999; Mulay *et al.* 1990; Halim *et al.* 1999). Studying the effect of doping on BSCCO system provides an opportunity to vary functional and mechanical properties of the material (Kazin *et al.* 1998). The dopant can influence kinetics and mechanism of HTSC phase formation, thus changing the final microstructure of the superconductor. In addition the dopant can form fine inclusions of stable phases serving as effective pinning centers. This method seems attractive for further improvement of critical current density in Bi(Pb)–2223 tapes (Ishizuka *et al.* 1995; Mao *et al.* 1997). The chemical routes such as oxalic acid coprecipitation, sol–gel (Shieh

et al. 1991) and micro–emulsion–based techniques (Kumar *et al.* 1993) are given priority to fabricate Bi(Pb)SrCaCuO powder in order to get high compositional homogeneity in such multi-component powder.

The importance of thermal property in physics is well known because it indicates the presence of phase transitions from a thermodynamic point of view (Bougrine *et al.* 2000). Thermal diffusivity is a measure of how quickly a temperature disturbance can propagate through a material and is related to thermal conductivity through the following equation

$$\alpha = \frac{\lambda}{\rho C_p} \tag{1}$$

This relationship allows the thermal conductivity (λ) to be calculated if thermal diffusivity (α), bulk density (ρ) and specific heat (C_p) are known. Photoflash method is one of the techniques that has been used intensively in determining the thermal diffusivity of solid sample. This technique, originally described by Parker *et al.* (1961) is a transient heat flow technique primarily used to measure the thermal diffusivity of the materials. The photoflash method involves rapidly heating one face of a small disk specimen with a single optical pulse and monitoring the temperature disturbance as a function of time on the other face of the specimen (Log and Jacson 1991). Then, the thermal diffusivity is calculated from a characteristic curve (thermogram) of the temperature excursion of its rear surface as

$$\alpha = \frac{1.38L^2}{t_{1/2}} \tag{2}$$

where L is the thickness of the sample and $t_{1/2}$ is the time required for the back surface of the specimen to reach half the maximum temperature rise.

In order to improve the superconducting properties of BSCCO, serious efforts have been made by changing chemical composition, conditions of sintering and annealing atmospheres, and doping with various cations. However, to the present knowledge, there is still lack of information for the effect of Sm doping upon the superconductivity of BSCCO prepared at different sintering time. The present paper describes the effect of doping composition and sintering time on the thermal diffusivity value for doped and undoped BSCCO superconducting ceramics.

EXPERIMENTAL SETUP

The experimental setup of photoflash technique is shown in *Fig.* 1. A normal electronic camera flash (Maxxum, model 5400HS) as an energy pulse source was positioned 2 cm from front surface of the sample. A disk-shaped sample was

placed on the sample holder and the K-type thermocouple was attached to the back surface of the sample. The front block of the sample was covered with the aluminium foil to shield the light from the photoflash reaching any part of the thermocouple.

In this setup, a fast response K-type thermocouple was attached directly to the rear surface of the sample to monitor the temperature at the rear surface of the sample. The signal from the thermocouple was then amplified by a preamplifier (SR560) and monitored by the digital oscilloscope (Tektronix TDS 220). The signal was then analyzed for thermal diffusivity value using equation (2). The photodiode (model RS 308(067) was used to trigger the oscilloscope. A period of 10 minutes was allowed in between the measurements in order to make sure the sample has reached the initial temperature (room temperature) before proceeding to a new measurement. For each sample, the measurements were repeated for more than three times.

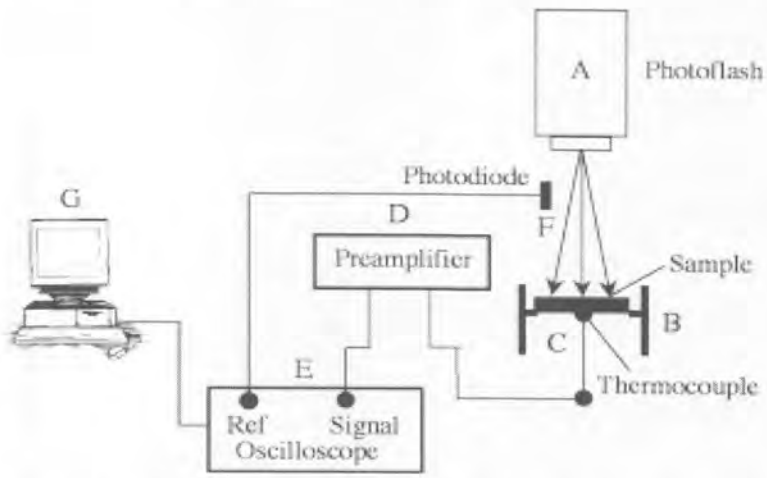

Fig. 1: Schematic experimental setup of the photoflash technique (A) light source, (B) sample holder, (C) thermocouple, (D) low noise preamplifier, (E) oscilloscope, (F) photodiode and (G) personal computer

SAMPLES PREPARATION

The general chemical stoichiometry for different substitutional doping in Bi–Pb–Sr–Ca–Cu–O system is shown in Table 1. The materials used in the preparation of $Bi_{1.6}Pb_{0.4}Sr_2Ca_2Cu_3O_\delta$ were metal acetates of bismuth, strontium, lead, calcium and copper, oxalic acid, deionized water and isopropanol. A stoichiometric amount of each component was weighed and dissolved in isopropanol– water solution with ratio 1: 1.5 at 0–2°C to produce a solution with a concentration of 0.5M. The solution was added to oxalic acid solution and stirred in an ice bath to obtain a uniform, stable and blue suspension. The final pH during the co–precipitation was between 2.0–2.5. The slurry was filtered off

after 5 minutes of reaction. The drying stage was carried out in the temperature range of 80–85°C for 8–12 h. The blue precipitate powder is slightly aggregated with particle size of 0.1–0.6 μm. The powder precursor was heated up to 730°C in air for 12 hours to remove the remaining volatile materials. The calcined powder was reground again and then pressed into pellets of ~ 12.5 mm diameter. The pellets were sintered at 850°C for 24, 48 and 100 hours and slow cooled to room temperature at a rate of 120°C/h. A similar procedure was repeated for $Bi_{1.6}Pb_{0.4}Sr_2Ca_2Cu_{3-X}Sm_XO_\delta$ (x = 0.02 – 0.4), and $Bi_{1.6}Pb_{0.4}Sr_{2-x}Sm_XCa_2Cu_3O_\delta$ (x = 0.02 – 0.4). The stoichiometric amount of each component was calculated and weighed to ensure a proper proportion of Sm^{3+} was used to dope in to the Cu or Sr site.

TABLE 1
Specimen formulation data for different substitutional doping in Bi-Pb-Sr-Ca-Cu-O system

Sample	Symbol	Dopant Sm, x
$Bi_{1.6}Pb_{0.4}Sr_2Ca_2Cu_3O_\delta$	BSCCO	0
$Bi_{1.6}Pb_{0.4}Sr_2Ca_2Cu_{3-x}Sm_XO_\delta$	BC1	0.02
	BC2	0.06
	BC3	0.1
	BC4	0.2
	BC5	0.3
	BC6	0.4
$Bi_{1.6}Pb_{0.4}Sr_{2-X}Sm_XCa_2Cu_3O_\delta$	BS1	0.02
	BS2	0.06
	BS3	0.1
	BS4	0.2
	BS5	0.3
	BS6	0.4

RESULTS AND DISCUSSION

Numerous corrections have been introduced to account for radiative heat losses during the process such as the finite width of the energy pulse and other factors which are interfering factors observed during the experiment. The effects of radiation heat loss at the rear surface were calculated from the transient response curve by employing the ratio technique. From this calculation, the heat loss occurred in the experiment were corrected using Clark and Taylor rise-curve technique (Maglic and Taylor 1992). The calculated ratio τ/t_c (pulse duration, τ = 5 ms for photoflash (Maxxum flash 5400HS)) from the experiment for the superconducting samples prepared at different sintering time showed that $\tau/t_c << 1$, therefore the finite pulse time effect in the present case is negligible (Cape and Lehman 1963).

TABLE 2
Thermal diffusivity values for pure $Bi_{1.6}Pb_{0.4}Sr_2Ca_2Cu_3O_\delta$ and Sm doped $Bi_{1.6}Pb_{0.4}Sr_2Ca_2Cu_3O_\delta$ superconductor ceramic sintered at 850 for various sintering time (24, 48 and 100 hours)

Material	$\alpha_c \times 10^{-3}$ (cm²/s) of Samples Sintered for 24 h	$\alpha_c \times 10^{-3}$ (cm²/s) of Samples Sintered for 48 h	$\alpha_c \times 10^{-3}$ (cm²/s) of Samples Sintered for 100 h
BSCCO	5.93 ± 0.07	5.93 ± 0.09	5.93 ± 0.09
BC1	7.36 ± 0.10	–	7.37 ± 0.10
BC2	8.99 ± 0.13	8.99 ± 0.12	8.98 ± 0.13
BC3	8.37 ± 0.11	8.37 ± 0.10	8.36 ± 0.12
BC4	6.51 ± 0.08	6.52 ± 0.12	–
BC5	5.56 ± 0.07	5.54 ± 0.07	5.55 ± 0.07
BC6	–	3.97 ± 0.04	–
BS1	7.76 ± 0.09	7.77 ± 0.11	7.77 ± 0.10
BS2	8.80 ± 0.14	8.81 ± 0.12	8.80 ± 0.13
BS3	8.09 ± 0.10	8.10 ± 0.11	8.08 ± 0.11
BS4	7.73 ± 0.10	7.71 ± 0.10	7.72 ± 0.10
BS5	–	7.05 ± 0.08	7.06 ± 0.09
BS6	6.76 ± 0.08	5.21 ± 0.06	5.22 ± 0.06

We first considered the effect of the sintering time of the doped and undoped BSCCO superconducting ceramic on thermal diffusivity. The doped and undoped BSCCO superconductors were sintered at 850°C with different sintering time (24, 48 and 100 hours). Table 2 shows the summary of thermal diffusivity values for doped and undoped BSCCO superconductor ceramics sintered at 850°C for 24, 48 and 100 hours. It was noted that the thermal diffusivity values remain unchanged, as the sintering time is increased. The independence of thermal diffusivity value with the sintering time for doped and undoped BSCCO system is clearly related to its microstructural characteristics. *Figs. 2-4* show the SEM micrographs of $Bi_{1.6}Pb_{0.4}Sr_2Ca_2Cu_3O_\delta$, $Bi_{1.6}Pb_{0.4}Sr_2Ca_2Cu_{3-X}Sm_XO_\delta$ and $Bi_{1.6}Pb_{0.4}Sr_{2-X}Sm_XCa_2Cu_3O_\delta$ prepared at various sintering time at magnification of 2300 times respectively. As the sintering time increased from 24 hours to 100 hours, the grain size for the sample remains the same. However, a change in the grain size was observed when the composition of dopant atom was changed.

The thermal diffusivity as a function of stoichiometric ratio of Sm, x for $Bi_{1.6}Pb_{0.4}Sr_2Ca_2Cu_{3-X}Sm_xO_\delta$ and $Bi_{1.6}Pb_{0.4}Sr_{2-X}Ca_2Cu_{3-X}Sm_xO_\delta$ sintered at 24, 48 and 100 hours is shown in *Fig. 5 (a)* and *(b)* respectively. It was noted that the thermal diffusivity for $Bi_{1.6}Pb_{0.4}Sr_2Ca_2Cu_{3-X}Sm_xO_\delta$ and $Bi_{1.6}Pb_{0.4}Sr_{2-X}Sm_XCa_2Cu_3O_\delta$ increased with the increase in dopant concentration to a maximum value at x = 0.06. Further increase in x resulted a decrease in the thermal diffusivity of $Bi_{1.6}Pb_{0.4}Sr_2Ca_2Cu_{3-X}Sm_xO_\delta$ and $Bi_{1.6}Pb_{0.4}Sr_{2-X}Sm_xCa_2Cu_3O_\delta$. These results indicate that the measured thermal diffusivity value of the BSCCO show strong

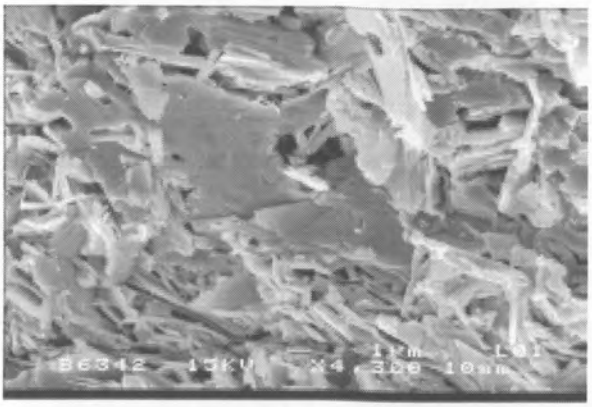

(a)

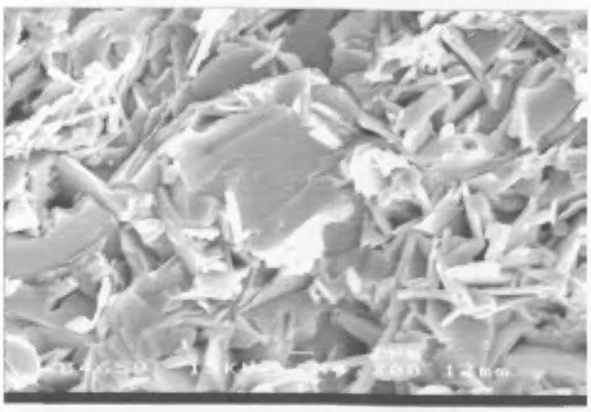

(b)

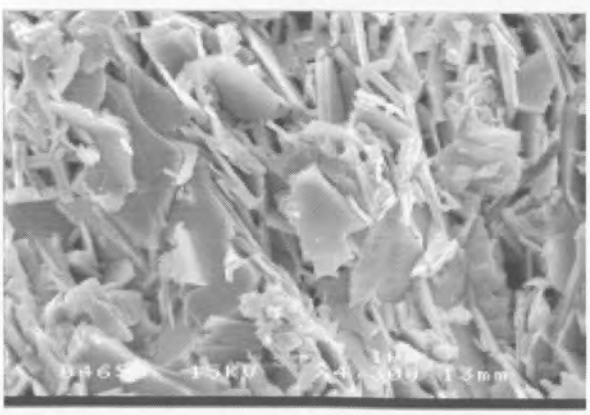

(c)

Fig. 2: SEM micrograph for $Bi_{1.6}Pb_{0.4}Sr_2Ca_2Cu_3O_\delta$ samples sintered at 850°C for (a) 24 hours (b) 48 hours (c) 100 hours

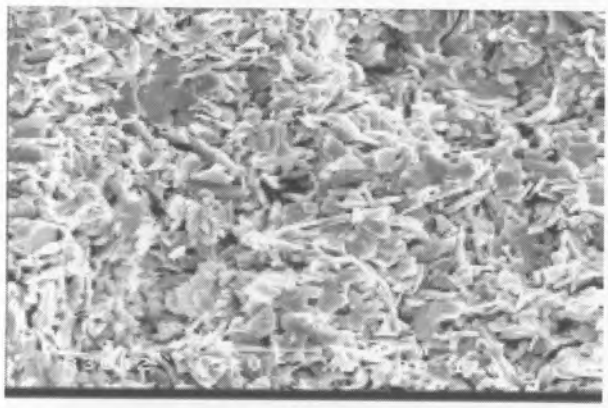

(a)

(b)

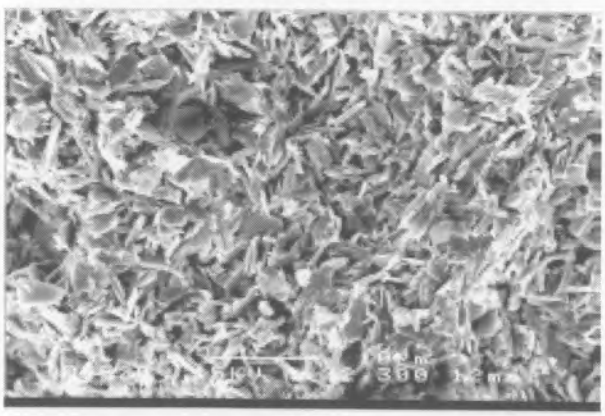

(c)

Fig. 3: SEM micrograph for $Bi_{1.6}Pb_{0.4}Sr_2Ca_2Cu_{3-X}O_\delta$ samples with x = 0.06 sintered at 850°C for (a) 24 hours (b) 48 hours (c)100 hours

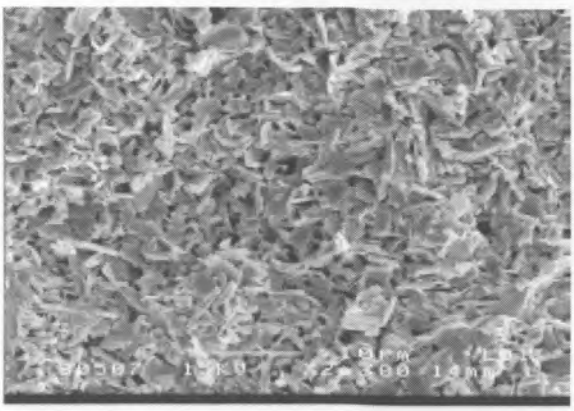

(a)

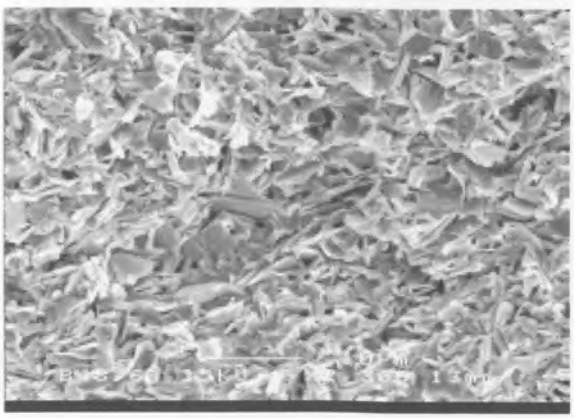

(b)

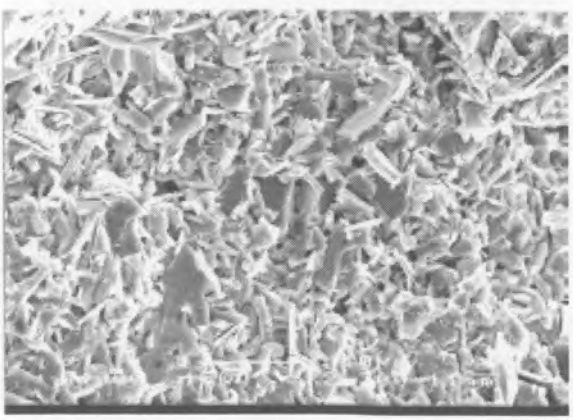

(c)

Fig. 4: SEM micrograph for $Bi_{1.6}Pb_{0.4}Sr_{2-X}Sm_xCa_2Cu_3O_\delta$ samples with x = 0.06 sintered at 850 for (a) 24 hours (b) 48 hours (c) 100 hours

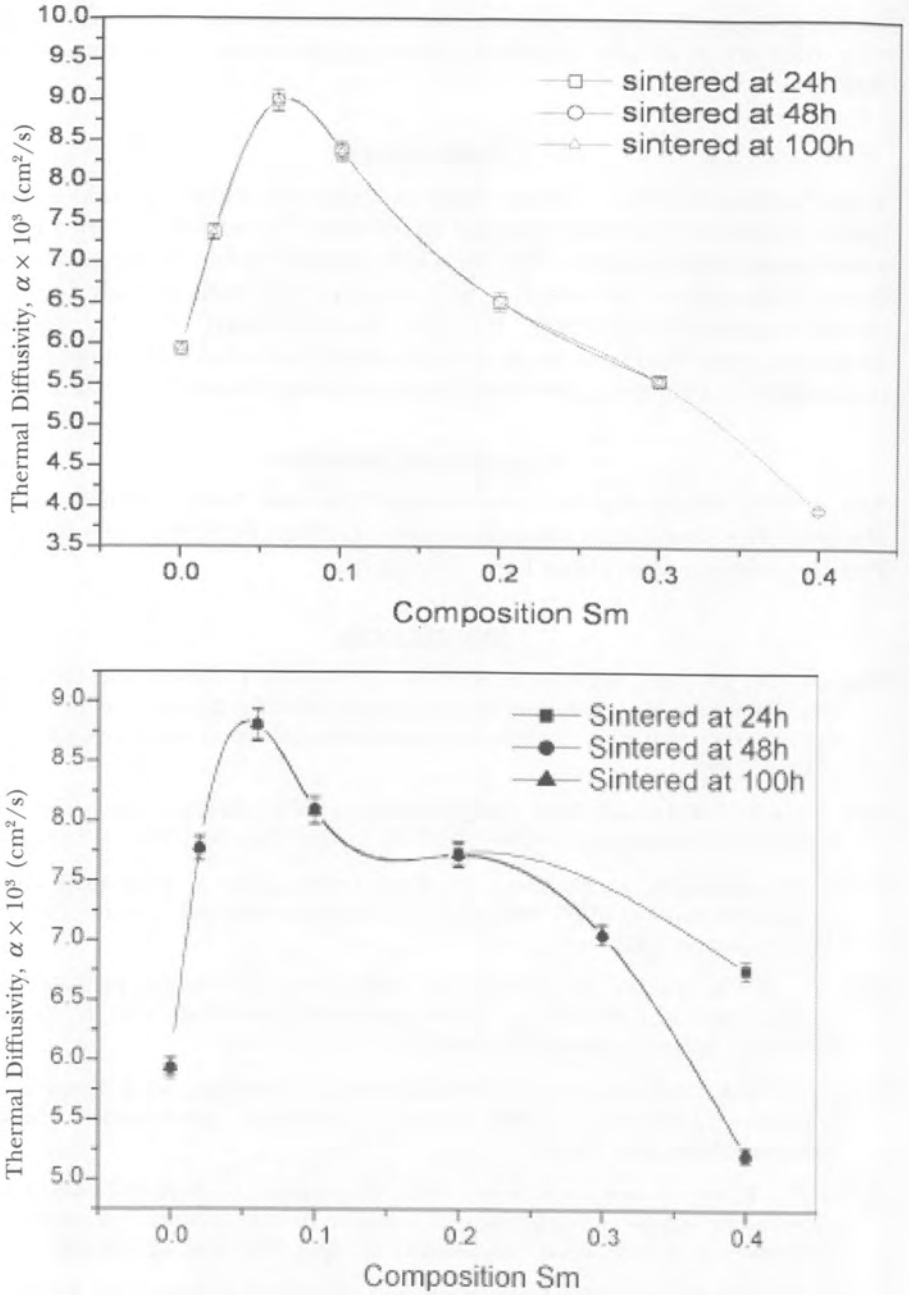

Fig. 5: Thermal diffusivity values versus composition of Sm for (a) $Bi_{1.6}Pb_{0.4}Sr_2Ca_2Cu_{3-X}Sm_xO_\delta$(b) $Bi_{1.6}Pb_{0.4}Sr_{2-X}Sm_xCa_2Cu_3O_\delta$ sintered at 850°C for various sintering time (24, 48 and 100 hours)

dependence on the dopant site and dopant concentration. However, sintering time does not show any significant effect on the room temperature thermal diffusivity.

CONCLUSION

It has been shown that a simple and inexpensive photoflash technique can be used to obtain the thermal diffusivity values of Sm doped and undoped BSCCO superconducting ceramics. The measured thermal diffusivity value was found to be independent of the sintering time of the sample but is strongly dependent on the dopant concentration. The SEM results indicated that the grain sizes could be a contributing factor to the thermal diffusivity as they showed similar dependence on sintering time and dopant concentration of the sample.

ACKOWLEDGEMENTS

The authors would like to acknowledge Universiti Putra Malaysia and the Malaysian Government for financial support through IRPA (09-02-04-0143) and PASCA programs (Josephine Liew Ying Chyi).

REFERENCES

Bougrine, H., J.F. Geys, S. Dorbolo, R. Cloots, J. Mucha, I. Nedkov and M. Ausloos. 2000. Simultaneous measurements of thermal diffusivity, thermal conductivity and thermopower with application to copper and ceramic superconductors. *Eur. Phys. J. B* **13:** 437-443.

Cape, J.A. and G.W. Lehman. 1963. Temperature and finite pulse-time effects in the flash methods for measuring thermal diffusivity. *J. Appl. Phys.* **34:** 1909-1913.

Halim, S.A., S.B. Mohamed, H. Azhan, S.A. Khawaldeh and H.A.A. Sidek. 1999. Effect of barium doping in Bi-Pb-Sr-Ca-Cu-O ceramics superconductors. *Physica C-Superconductivity* **312:** 78-84.

Ishizuka, M., Y. Tanaka and H. Maeda. 1995. Superconducting properties and microstructures of Bi-2223 Ag-Cu alloy sheathed tapes doped with Ti, Zr or Hf. *Physica C - Superconductivity* **252:** 339-347.

Kazin, P.E., M.A. Uskova, Yu, D. Tretyakov, M. Jansen, S. Scheurell and E. Kemnitz. 1998. Formation of Bi(Pb)-2223 with chemically compatible V-rich phase. *Physica C-Superconductivity* **301:** 185-191.

Kumar, P., V. Pillai and D.O. Shah. 1993. Preparation of Bi-Pb-Sr-Ca-Cu-O oxide superconductors by coprecipitation of nanosize oxalate precursor powders in the aqueous core of water-in-oil microemulsions. *Appl. Phys. Lett.* **62:** 765-767.

Log, T. and T.B. Jackson. 1991. Simple and inexpensive flash technique for determining thermal diffusivity of ceramics. *J. Am. Ceram. Soc.* **74:** 941-944.

Maglic, K.D. and R.E. Taylor. 1992. The apparatus for thermal diffusivity measurement by the laser pulse method. In *Compendium of Thermophysical Property Measurement Methods*, **2**: 281-314. New York, London: Plenum Press.

MAO, C., L. ZHOU, X. SUN and X. WU. 1997. Coprecipitation-based micro-reactor process to synthesize soft-agglomerated ultrafine BiPbSrCaCuO powder with low carbon content. *Physica C - Superconductivity* **281:** 35-44.

MOLLAH, S. 2002. Critical temperatures and critical currents of PbBiSCCO–metal/alloy composites. *Mater. Letts.* **52:** 159-165.

MULAY, V.N., P.V.L.N. SIVA PRASAD, K. BHUPAL REDDY and M.A. JALEEL. 1990. Studies on the synthesis of Bi2Ca1Sr2Cu2O8 by different chemical routes. *J. Mat. Sci. Lett* **9:** 1284-1287.

PARKER. W.J., R.J. JENKINS, C.P. BUTLER and G.L. ABBOTT. 1961. Flash method of determining thermal diffusivity, heat capacity, and thermal conductivity. *J. Appl. Phys.* **32:** 1679-1684.

SHIEH,, C.Y., Y. HUANG, M.K. WU and C.Y. HUANG. 1991. Preparation of single high-Tc phase Bi-Pb-Sr-Ca-Cu-O superconductor by the EDTA precursor solution method. *Physica C- Superconductivity* **185-189:** 513-514.

TRONG O. D., O. SATO, A. FUJISHIMA and K. HASHIMOTO. 1999. Change of the critical temperature of high Tc single (2223) phase Bi-Pb-Sr-Ca-Cu-O superconductors by intercalation process. *J. Phys. Chems. Solids* **60:** 883-890.

Pertanika J. Sci. & Technol. **14(1 & 2)**: 13 - 32 (2006)
ISSN: 0128-7680

Purchasing Power Parity Revisit: A Comparison of Linear and Nonlinear Models

***Ahmad Zubaidi Baharumshah & Hooy Chee Wooi**
Department of Economics,
Faculty of Economics and Management,
Universiti Putra Malaysia,
43400 UPM, Serdang, Selangor, Malaysia

Received: 14 October 2003

ABSTRAK

Kajian ini cuba memperkembangkan isu Pariti Kuasa Beli (PPP) dari dua sudut. Pertama, perbandingan dibuat antara model fungsi linear PPP (OLS) dengan model fungsi tidak linear PPP (GARCH). Kedua, isu PPP diselidik semula menggunakan data yang terkini dari Januari 1980 hingga November 2002, termasuk krisis kewangan Asia untuk lima buah negara ASEAN. Keputusan empirikal mencadangkan bahawa matawang ASEAN-5 kembali ke keseimbangan nilai PPP di dalam jangka masa yang panjang. Matawang Peso Filipina dan Dollar Singapura menerima impak yang kurang daripada krisis matawang. Walaupun, Malaysia dan Thailand mengalami penurunan matawang yang besar, kedua-dua matawang tersebut kembali ke keseimbangan asal pada jangka masa yang lebih singkat daripada matawang yang lain. Selain itu, sifat tidak linear matawang ASEAN-5 juga didokumentasikan dalam kajian ini. Ini diperkuatkan dengan pencapaian yang lebih baik oleh model fungsi tidak linear daripada model fungsi linear dari segi penghasilan ramalan pertukaran asing dalam memodelkan PPP.

ABSTRACT

This paper aims to expand PPP literature by twofold. First, the performance of the conventional linear PPP model (OLS) is compared with nonlinear PPP (GARCH). Secondly, we revisit the PPP by using more recent data for the currencies of five leading members of the Association of Southeast Asia Nations (ASEAN-5), covering from January 1980 to November 2002, including the recent Asian financial crisis. Our results suggest that generally, the ASEAN-5 currencies still revert to their PPP equilibrium over long run time horizon. While all series show response to the crisis, the Philippine peso and Singapore dollar obviously received the least impact. Although Malaysia and Thailand have suffered huge undervaluation during the crisis, both Malaysian ringgit and Thai baht are found to be corrected at a quicker pace relative to the other three currencies from the misalignments. In addition, we also documented several nonlinear behaviors of the ASEAN-5 currencies and found that the nonlinear models outperform the linear model in modeling PPP, based on their superiority in out-of-sample forecasting.

Keywords: PPP, GARCH, EGARCH-M, forecasting

* Corresponding author:
E-mail: *zubaidi@putra.upm.edu.my*

INTRODUCTION

Long since the early of last century, purchasing power parity (PPP) has been viewed as centre of exchange rate determination, as well as basis for international capital flow theories. Put simply, the PPP approach states that the exchange rate between two national currencies should move to equate the prices of an identical bundle of goods produced in the two countries. Thus, the equilibrium real exchange rate is predicted to be constant. If the current exchange rate deviate from its PPP equilibrium, there is an opportunity for arbitrage in the goods and capital markets, which will tend to drive the exchange rate towards the PPP.

While PPP is a simple and powerful idea, it has fallen out of fashion as a tool to forecast exchange rate for practitioners due to two reasons. First, exchange rate is driven not only by price or inflation differentials, as presumed by the PPP approach, but also by a wide range of other money and non-money factors, such as political stability, relative productivity, and demand shock, to name just a few. This has leads to the second reason, where most empirical studies documented that the PPP only holds (at best) over very long time horizons. In the short and medium term, exchange rate tends to deviate substantially from PPP due to shocks from the above mentioned money and non-money factors; suggesting a volatility persistency phenomenon. This is why most market analysts and practitioners usually reject the PPP approach to exchange rate determination.

Scholarly research as well, is not favorable to PPP. Since the hallmark work of Meese and Rogoff (1983), the naïve random walk model has tried to snub PPP both theoretically and empirically. The bulk of recent literature as well, fails to achieve a consensus to accept the PPP, even as a long run relationship. Academicians are still attempting to find new empirical facts by exploiting new techniques and models that are able to capture the dynamic nature of exchange rate. Recently, there is ample evidence against the linear paradigm, showing that financial time series are more likely to exhibit nonlinear dependencies (e.g. exchange rate, inflation, stock returns and interest rate parity)[1]. With this development, the subject has moved to a new direction, which is, of course, the incorporations of non-linearity in the PPP model. For example, nonlinear models such as Neural Network (NN) approaches, Threshold Autoregressive (TAR), Generalized Autoregressive Conditional Heteroscedasticity (GARCH) family of models, and Smooth Transition Autoregressive (STAR) family of models, are all widely employed in recent papers to explain the dynamic of financial time series especially the exchange rate (See for example, Liew *et al.* 2004; Sarno 2000a,b; Vilasuso 2002; Baillie and Bollerslev 1991)[2].

---

[1] There is a growing consensus among the profession that attempts to examine fundamental topics within finance will be less well specified, and hence, less informative, if they rely on traditional linear modeling approaches.

[2] An excellent summary on the asymmetric GARCH models is found in Hentschel (1995)).

This paper aims to expand the current interest by twofold. First, the performance of the conventional linear PPP model is compared with the GARCH model advanced by Bollerslev (1986). To date, there is a lack of GARCH-based PPP literature because the standard way of PPP research is by large using the unit root and cointegration tests. Second, we revisit PPP doctrine by using more recent data for the currencies of five leading members of the Association of Southeast Asia Nations (ASEAN-5), covering from January 1980 to November 2002. This is important for the reason that nearly all of the published works focus on data up to 1998, excluding the Asian financial crisis (e.g. Baharumshah and Ariff 1997; Sazanami and Yoshimura 1999; Azali *et al.* 2001). We intend to investigate whether the recent crisis has left a significant impact on the long run PPP by using a crisis dummy.

Our results suggest that generally, the ASEAN-5 currencies still revert to PPP over long run time horizon. While the Philippine peso and Singapore dollar received the least impact from the recent crisis, both the Malaysian ringgit and Thai baht are found to have smaller cycle of PPP misalignments. In addition, we also documented several nonlinear behaviors of the ASEAN-5 currencies and found that the nonlinear models outperform the linear model, based on their superiority in out-of-sample forecasting.

This paper is organized as follow; section 1 serves as introduction; section 2 provides the literature review; this is followed by section 3, methodology and data; section 4 reports the empirical results, where the analysis is carried out in three stages - modeling of the linear and nonlinear PPP, conducting unit root test on the real exchange rates, and a comparison of within and out-of-sample forecasting performance of both types of models. The final section offers the concluding remarks.

LITERATURE REVIEW

Studies on exchange rate and its determination have received a lot of attention in the literature.[3] The central of all theory of exchange rate models are based on some form of PPP. Nevertheless, most of the empirical works have failed to reject the null hypothesis of a unit root in exchange rate. In spite of the use of numerous statistical techniques over sample periods ranging to 25 years, there has been little evidence to support the PPP hypothesis for the developing countries. For example, the article by Bahmani-Oskooee (1993) overwhelming rejects the stationarity of real exchange rates for most of the LDCs[4]. That is to say, in our present context, real exchange rates in these countries are persistent over the generalized floating exchange rate period. Similar findings were also documented in, for example, Gan (1991) for Malaysia; in Baharumshah and Ariff (1997) for the ASEAN-5 countries (ASEAN-5: Malaysia, Indonesia, Thailand,

[3] For survey on the early theoretical development on exchange rate determination, please see Macdonald and Taylor (1992) and Taylor (1995).

[4] Bahmani-Oskooee (1993) found that PPP holds for only four out o twenty-five developing countries.

Singapore and the Philippines), and in Aggarwal and Mougoue (1996) for the Asian Tigers and the ASEAN countries[5].

The failure to confirm PPP means that standard models used to determine exchange rate movements (and policy guidance) may therefore yield misleading results, as deviations from the PPP tends to be persistent and real exchange rate follows a random walk process[6]. In other words, policy guidance that is based on PPP is questionable. It is worth noting that the empirical literature suggests that a number of reasons for the failure to reject the nonstionarity of real exchange (PPP does not hold). However, two main arguments dominate. The first is that the span of available data was simply too short to provide reasonable power in the conventional tests used for nonstatinary (see Sarno (2000a,b) and Liew *et al.* (2004). The second was that real exchange rate was determined by real factors (oil shocks, productivity differentials and fiscal variables (see Rogoff (1996) and MacDonald (1997))[7].

Current research in exchange rate modeling attests that real exchange rate exhibit nonlinear dependencies in its adjustment to PPP. Hsieh (1989), Caporale and Pittis (1996), Brooks (1996), Brooks (1997), Choo *et al.* (2001), Lim *et al.* (2002) and Liew *et al.* (2004) have provided ample evidence on the exchange rates nonlinearity. In this regard, many nonlinear models have emerged to provide alternative dimension in reviewing the judgment place on PPP. Brooks (1997) for example, found that the parsimonious Neural Network (NN) and GARCH type of models do perform better in modeling the exchange rates movement. Nevertheless he reserves the full superiority of such models to capture the stochastic exchange rates dynamic and suggests that a time-varying coefficients model would be ideal. Choo *et al.* (2001) as well, have documented the success of GARCH-type of models to outperform the naïve random walk model in out-of-sample forecasting. Caporale and Pittis (1996) and Liew *et al.* (2002) on the other hand, suggest that the STAR model is well equipped to handle nonlinearity in exchange rates.

Indeed, recent work on alternative linear and nonlinear econometric modeling has re-energized empirical evidence on PPP. Baharumshah (2002) has provided a comprehensive discussion on both linear and nonlinear paradigm of the PPP for East Asia currencies, and seeing nonlinearity as a complement to long run PPP to withhold. Azali *et al.* (2001) for example, found evidence for the PPP to hold for seven Asian developing economies (ADE) with Japan, from 1977 to 1998. More recently, Taro (2002), using a panel of 13 disaggregated CPI (1960-1998) from seven major Japan cities, also supports for the PPP across

---

5 For the case of the developed countries and the major currencies, the reader may refer to Engle (2000) and the articles cites therein.

6 Failure of PPP is also consistent with a related line of study that have reported the half-life (the speed at which that deviation from PPP die out) is far to high (3-5 years) to be explained by existing theoretical model

7 The famous Balassa-Samuelson effect arises when relative factor proportions and factor prices become imbalance due to relative differences in the rate of technological shock.

cities. Papell 's (2002) structural change panel approach as well rejects most of the unit root null, though not all in their study of 20 industrialized countries from 1973-1996. Additionally, Liew *et al.* (2002) found that the PPP withhold for ASEAN-5 and Korea in the period spans from 1968 to 2001. In short, the development of the nonlinear models (e.g. NN, GARCH, TAR, STAR), KPSS, panel unit root and panel cointegration tests, have dominated the research trend, and provide researcher an opportunity in attempting to prove the PPP using data from the current float.

MODELING STRATEGY AND THE DATA

The empirical test for a long run PPP is typically based on the following equation:

$$s_t = a + b_1 p_t + b_2 p_t^* + \varepsilon_t \quad (1)$$

where s_t is the logarithm of the nominal exchange rate in period t, defined as domestic price of foreign currency p_t, the logarithm of domestic price, p_t^* the logarithm of foreign price, a, b_1, and b_2 are the parameters, and ε_t is the error term. The restriction commonly imposed on the parameters are, $a = 0$, $b_1 = 1$ and $b_2 = -1$. With these restrictions, the error term is a measure of the deviation of real exchange rate, where:

$$\varepsilon_t \equiv s_t - p_t + p_t^* \quad (2)$$

If the PPP holds, the long-run movement of s_t, p_t and p_t^* cancels out, that is, s_t, p_t and p_t^* are cointegrated. To test for the stationarity of the real exchange rate, we applied the conventional Augmented Dickey Fuller (ADF) test on the residuals ε_t. In addition, to capture the effect of the recent financial crisis, a dummy variable (D_{crisis}) is added to equation (1) to yield:

$$s_t = a + b_1 p_t + b_2 p_t^* + cD_{crisis} + \varepsilon_t \quad (3)$$

where c measures the impact of the crisis. Equation (3) is estimated by using the Ordinary Least Square (OLS) method. To conserve space, we do not discuss the details of the tests here.

In this paper, two nonlinear models (Generalized Autoregressive Conditional Heteroscedasticity or simply GARCH) are proposed. The GARCH-type of models are proposed because they are capable to capture the excess kurtosis and volatility clustering behavior of the exchange rate. A conventional symmetrical GARCH (1,1) model and an asymmetrical Exponential GARCH

(1,1) in Mean (EGARCH-M) model are fitted to PPP, as given respectively by equation (4), (5), (6) and (7)[8] as follows:

GARCH (1, 1) (symmetrical):

$$s_t = \mu + \delta_1 p_t + \delta_2 p_t^* + cD_{crisis} + \nu_t \tag{4}$$

$$h_t = \omega + \beta h_{t-1} + \alpha\varepsilon_{t-1} + \theta D_{crisis} \tag{5}$$

EGARCH (1, 1)-M (asymmetrical):

$$s_t = \mu + \delta_1 p_t + \delta_2 p_t^* + \tau\sqrt{h_t} + cD_{crisis} + \nu_t \tag{6}$$

$$\log h_t = \omega + \beta \log h_{t-1} + \alpha\left|\frac{\nu_{t-1}}{\sqrt{h_{t-1}}}\right| + \gamma\frac{\nu_{t-1}}{\sqrt{h_{t-1}}} + \theta D_{crisis} \tag{7}$$

where h_t represents the conditional variance of the residual term. μ, δ_1, and δ_2 are the parameters in the conditional mean of the exchange rate, and ν_t is the error term. The parameters in the conditional variance are given respectively by ω, α and β. The parameter θ is the coefficient measuring the impact of the recent crisis on the volatility of the exchange rate.

The EGARCH-M model has an added advantage to account for the leptokurtosis in financial time series and this enables us to test for the leverage effect of bad news. The asymmetrical effect is detained by γ.[9] The model is expected to perform better in the uncertainty (volatility) period, as it could differentiate the effects of good and bad news in the market. In addition, EGARCH-M also considers the possibility of a conditional volatility feedback effect in the exchange rate, where the coefficient of the volatility feedback is represented by the parameter τ.

The data employed in this study covered the monthly bilateral exchange rate and consumer price index (CPI) from January 1980 to November 2002.[10]

---

8 The theoretical model used most studies is based on PPP relationship. The bulk of the literature has demonstrated that PPP failed to hold in the short-run. Besides that, it is well known that the out-sample forecasts generate from simple random walk model usually outperformed structural models at short horizon. In other words, random walk tends to dominate PPP point prediction at short forecasting horizon. The predictive content of structural models like PPP are expected to significantly improve as the forecasting horizon is lengthen. We are grateful to one of the referees for pointing out his to us.

9 The response of the PPP model (conditional volatility) to good and bad news are asymmetry if $\gamma \neq 0$ the variance equation (7), the impact is symmetry if $\gamma = 0$. The presence of the leverage effects can be tested by the hypothesis of $\gamma < 0$.

10 The appropriate price index should cover goods that are traded internationally. Several authors have argued that the producer price index (PPI) is a better choice that the CPI. But monthly data for PPP spanning over the sample period for all the countries under investigation is unavailable for this study.

Following the common practice in the literature, all the series are expressed in logarithm. The data are collected from the IMF International Financial Statistics (IFS), various issues. The sample covers the CPI of the US and ASEAN-5; and the currencies of Indonesia rupiah, Malaysian ringgit, Philippine peso, Singapore dollar and Thai baht. ASEAN-5 is chosen because of the growing importance of ASEAN in the world economy both in terms of trade and investments. The implementation of the Asia Free Trade Area (AFTA) in 2005 has prompted this region to progress competitively. Yet the linkages among the ASEAN members have not gained much attention in the literature.

THE PPP MODELING AND FORECASTING

Table 1 presents the summary statistics for all the exchange rates and CPI series involved. Table 2, table 3 and table 4 provide the parameter estimation of PPP based on the linear OLS, nonlinear symmetrical GARCH, and nonlinear asymmetrical EGARCH-M respectively. Table 5 reports the unit root test based on ADF, while table 6 summarizes the within sample and out-of-sample forecasting comparison of the three models. We note that the lag lengths for the ADF test are chosen based on the Akaike (AIC) and Schwaz (SIC) information criteria.

A quick glance on the parameter estimation of all three PPP models seem to promise a good-fitted model (85% parameters are significant). R^2 are fairly high for all the fitted series (over 90%), except the Singapore dollar. Nevertheless, the coefficient values of the CPI are not satisfactory to withhold PPP. A further test on the price ratios using the Wald test also shows that the common PPP restriction of negative unity can be rejected at a 1% significant level.

An interesting finding however, has been documented for the crisis's dummy. The dummy variable (c) turned out to be significant in all the models, except Indonesian rupiah in EGARCH-M modeling. The exclusion of the step dummy (takes value of 1 in 1997: 07-1998: 12) in most cases yielded non-normal residuals. The Philippine peso and Singapore dollar obviously received the least impact from the crisis, by observing the coefficient values. Both the currencies together with the Thai baht, also show insignificant θ values in the nonlinear modeling, except Singapore dollar in EGARCH-M modeling, indicating that the volatility of exchange rate of these countries are not affected significantly by the currency crisis.

Volatility persistency has been a dominant trend in ASEAN-5 currencies, as a high percentage of conditional variance's variables are statistically significant. This shows that nonlinearity does exist in the PPP model and it is successfully captured by the GARCH model. The EGARCH-M model further provides evidence for asymmetrical news effect and volatility feedback effect but the leverage effect only happened in the Malaysian ringgit and Philippine peso.

Figs. 1, 2 and *3* show the implied misalignments of ASEAN-5 currencies against the US dollar. It is measured by the deviations of ASEAN-5 nominal exchange rates from the equilibrium PPP rates generated by OLS, GARCH, and EGARCH-M respectively. A positive deviation indicates undervaluation while a negative deviation means overvaluation. It appears that there were serious

TABLE 1
Summary statistics for all series

	Nominal Exchange Rates					Consumer Price Index					
	Indonesia	Malaysia	Philippine	Thailand	Singapore	US	Indonesia	Malaysia	Philippine	Thailand	Singapore
Mean	7.675	1.014	3.120	0.601	3.324	4.448	4.368	4.478	4.172	4.505	4.431
Median	7.578	0.946	3.230	0.589	3.240	4.491	4.254	4.456	4.295	4.514	4.426
Maximum	9.609	1.519	3.981	0.820	4.006	4.779	5.678	4.795	5.046	4.665	4.844
Minimum	6.438	0.757	2.004	0.329	3.016	3.934	3.278	4.071	2.838	4.220	3.855
Std. Dev.	0.864	0.186	0.539	0.145	0.228	0.226	0.672	0.201	0.651	0.119	0.277
Skewness	0.550	0.987	-0.580	-0.275	1.070	-0.333	0.461	0.017	-0.490	-0.242	0.050
Kurtosis	2.379	2.556	2.743	1.853	2.862	1.958	2.142	1.880	2.129	1.876	1.715
Jarque-Bera	18.283	46.901	16.192	18.554	52.692	17.519	18.160	14.388	19.725	17.145	19.025
Probability	0.000	0.000	0.000	0.000	0.000	0.000	0.000	0.001	0.000	0.000	0.000
Observations	275	275	275	275	275	275	275	275	275	275	275

TABLE 2
OLS estimation results

Model: $s_t = a + b_1 p_t + b_2 p_t^* + cD_{crisis} + \varepsilon_t$

ASEAN 5	Parameters				R^2	*LogL*	b_1/b_2	*F-statistics*
	a	b_1	b_2	*c*				
Indonesia	2.004 (0.003)***	0.922 (0.000) ***	0.347 (0.1812)	0.453 (0.000) ***	0.950	86.577	2.657	182.289 (0.000) ***
Malaysia	0.842 (0.000)***	-0.937 (0.000) ***	0.961 (0.000) ***	0.404 (0.000) ***	0.914	404.247	-0.975	865.681 (0.000) ***
Philippine	5.791 (0.000)***	1.385 (0.000) ***	-1.908 (0.000) ***	0.101 (0.000) ***	0.948	189.590	-0.726	25.452 (0.000) ***
Singapore	7.540 (0.000)***	-1.674 (0.000) ***	0.126 (0.1947)	0.161 (0.000) ***	0.852	359.785	-13.286	180.580 (0.000) ***
Thailand	1.826 (0.000)**	-0.911 (0.000) ***	1.216 (0.010) ***	0.504 (0.000) ***	0.920	378.956	-0.749	201.851 (0.000) ***

Log L is the log-likelihood functions value. The common PPP restriction of b_1/b_2=-1 is tested by the Wald test and reported under the *F-statistics*. Values in the parentheses are the p-values. * denotes significance at 0.10 level; ** denotes significance at 0.05 level and *** denotes significance at 0.01 level. All the time series are measured in the logarithmic form.

TABLE 3
GARCH (symmetrical) estimation results

Model: $s_t = \mu + \delta_1 p_t + \delta_2 p_t^* + cD_{crisis} + v_t$; $h_t = \omega + \beta h_{t-1} + \alpha\varepsilon_{t-1} + \theta D_{crisis}$

	Parameters					
ASEAN 5	μ	δ_1	δ_2	c	R^2	*LogL*
Indonesia	0.917 (0.000)***	0.751 (0.000) ***	0.761 (0.000) ***	0.478 (0.000) ***	0.948	226.409
Malaysia	1.222 (0.000)***	-1.165 (0.000) ***	1.103 (0.000) ***	0.451 (0.000) ***	0.910	550.222
Philippine	5.812 (0.000)***	1.403 (0.000) ***	-1.918 (0.000) ***	0.028 (0.0344) **	0.939	281.429
Singapore	7.775 (0.000)***	-1.694 (0.000) ***	0.093 (0.000) ***	0.175 (0.000) ***	0.849	501.038
Thailand	2.151 (0.000)***	-0.933 (0.000) ***	1.162 (0.000) ***	0.493 (0.000) ***	0.902	581.938
	ω	α	β	θ	δ_1 / δ_2	*F-statistics*
Indonesia	1.56E-05 (0.344)	1.187 (0.000) ***	0.112 (0.148)	0.006 (0.029) **	0.987 (0.000) ***	31657.12
Malaysia	9.50E-05 (0.000) ***	0.985 (0.000) ***	-0.037 (0.456)	0.006 (0.000) ***	-1.056 (0.000) ***	4372.36
Philippine	0.001 (0.003) ***	1.095 (0.000) ***	-0.0715 (0.000) ***	4.00E-04 (0.622)	-0.731 (0.000) ***	131.07
Singapore	1.03E-04 (0.000) ***	1.108 (0.000) ***	-0.068 (0.201)	0.001 (0.354)	-18.215 (0.000) ***	14230223
Thailand	2.74E-05 (0.000) ***	1.218 (0.000) ***	-0.022 (0.571)	3.58E-04 (0.121)	-0.803 (0.000) ***	131372.10

misalignments of the ASEAN-5 currencies from the linear and nonlinear PPP equilibrium rates prior crisis. An interesting occurrence is that the Indonesian rupiah, Malaysian ringgit, and Thai baht all depict a sharp overvaluation prior to the outburst of the crisis. As expected, the asymmetrical EGARCH-M model captured the sharp overvaluations.

The crisis and the degree of its impact are shown by the sharp undervaluation received by ASEAN-5 currencies. The linear and nonlinear models all show that

TABLE 4
EGARCH-M (asymmetrical) estimation results

Model: $s_t = \mu + \delta_1 p_t + \delta_2 p_t^* + \tau\sqrt{h_t} + cD_{crisis} + v_t$; $\log h_t = \omega + \beta \log h_{t-1} + \alpha\left|\frac{v_{t-1}}{\sqrt{h_{t-1}}}\right| + \gamma\frac{v_{t-1}}{\sqrt{h_{t-1}}} + \theta Dcrisis$

	Parameters						
ASEAN 5	μ	δ_1	δ_2	τ	c	R^2	*LogL*
Indonesia	-4.132	0.472	2.074	7.755	0.004	0.983	391.999
	(0.000)***	(0.011) **	(0.000) ***	(0.000) ***	(0.449)		
Malaysia	-1.332	0.716	-0.176	-5.167	0.323	0.947	589.331
	(0.000)***	(0.000) ***	(0.127)	(0.000) ***	(0.000) ***		
Philippine	5.865	1.409	-1.925	-0.947	0.062	0.957	325.340
	(0.000)***	(0.000) ***	(0.000) ***	(0.000) ***	(0.000) ***		
Singapore	7.983	-1.692	0.039	0.479	0.201	0.780	500.467
	(0.000)***	(0.000) ***	(0.002) ***	(0.000) ***	(0.000) ***		
Thailand	0.657	-0.736	1.282	6.877	0.201	0.976	650.084
	(0.000)***	(0.000) ***	(0.000) ***	(0.000) ***	(0.001) ***		
	ω	α	β	γ	θ	δ_1 / δ_2	*F-statistics*
Indonesia	-0.313	0.030	0.956	0.367	0.226	0.228	691.547
	(0.000)***	(0.196)	(0.000) ***	(0.000) ***	(0.001) ***		(0.000) ***
Malaysia	-0.399	0.062	0.957	-0.256	0.158	-4.068	480.814
	(0.026)**	(0.013) **	(0.000) ***	(0.000) ***	(0.012) **		(0.000) ***
Philippine	-2.012	1.326	0.839	-0.464	0.181	-0.732	297.324
	(0.000)***	(0.000) ***	(0.000) ***	(0.001) ***	(0.331)		(0.000) ***
Singapore	-2.640	1.601	0.809	0.499	0.136	-43.385	9823.051
	(0.000)***	(0.000) ***	(0.000) ***	(0.003) ***	(0.000) ***		(0.000) ***
Thailand	-0.784	-0.143	0.899	0.330	0.332	-0.574	241.083
	(0.000)***	(0.000) ***	(0.000) ***	(0.000) ***	(0.478)		(0.000) ***

the undervaluation hit Indonesia the most, followed by Thailand and Malaysia, while Singapore is apparently least affected from the contagion effect, where the undervaluation is small. Nevertheless, Singapore dollar, Thai baht and Philippine peso are all undervalued after the new millennium, as shown consistently by both the linear and nonlinear models. The Malaysian ringgit however, has converged to the PPP equilibrium after the pegging to the US dollar.

An overview of PPP adjustment of the ASEAN-5 currencies across the whole sample period provides an interesting finding. Clearly, the misalignments of Malaysian ringgit and Thai baht tend to be corrected more quickly relative to others. The Malaysian ringgit and Thai baht had followed the PPP since the 1980s, except a distortion from the Asian financial crisis. The pattern is even apparent under the EGARCH-M model. Although the Singapore dollar and Philippine peso also show convergent to PPP across the period, the patterns of convergent are not so obvious and the cycle of adjustment is relatively larger than the Malaysian ringgit and Thai baht. The Indonesian rupiah on its own, shows inconsistent alignment from the PPP as indicated in the linear OLS and nonlinear GARCH models. Under the EGARCH-M modeling however, the Indonesian rupiah seems to follow the PPP nicely until the Asian financial crisis.

The results of the ADF unit root test in Table 5 show positive evidence for the PPP hypothesis. In the standard linear model, there was evidence of PPP relationships (a) between Malaysia and US, (b) between Singapore and US, (c) between Thailand and US, (d) between Indonesia and US, and (e) between Philippines and US. The hypotheses of unit root are also rejected at conventional significance levels for the GARCH-type models, showing a cointegrating vector exist between price and exchange rate, except for the Philippine peso. The PPP between the Philippines and US only holds in the asymmetrical EGARCH-M model. In short, the results indicate that the ASEAN-5 real exchange rates are stationary (or mean reverting), at least for the sample period considered in this study. The rates adjust in the short run, in a fashion to restore the long-run equilibrium relationship.

Multinational corporations aim to establish and extend their businesses in the fast growing East Asia emerging markets, including the large ASEAN countries. The recent currency crisis in Asia highlights the instability of these growing economies and stresses that firms need to closely scrutinize the foreign exchange markets. For large corporations which conduct substantial currency transfers, being able to accurately forecast the movements of the exchange rate is important in order to manage exchange rate risk. It is worth noting here that the predictive performance of exchange rate models has not been seriously undertaken in past studies. Hence, we now turn to the predictive performance of the PPP model in forecasting the ASEAN currencies against the US dollar.[11]

[11] Evaluation of the forecastibility of the ASEAN currencies based on the structural model would complement the existing literature on exchange rate models which have focused mainly on the major currencies—US dollar, German mark and the Japanese yen.

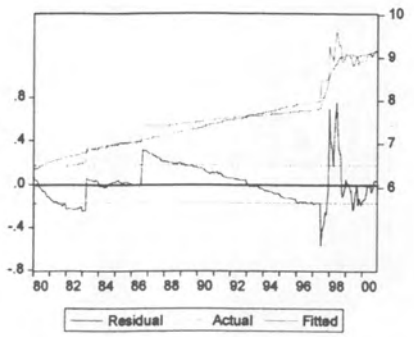

Indonesia

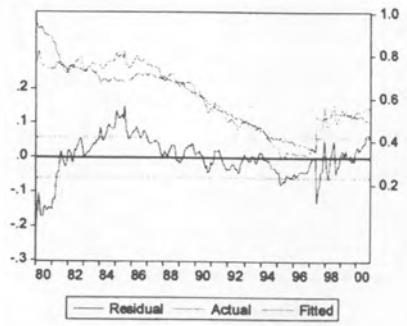

Singapore

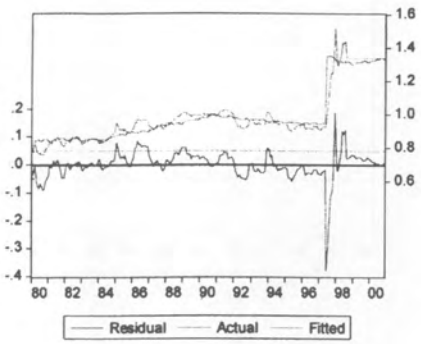

Malaysia

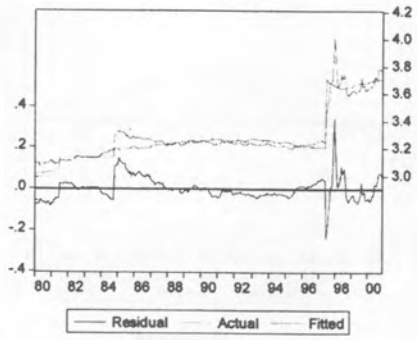

Thailand

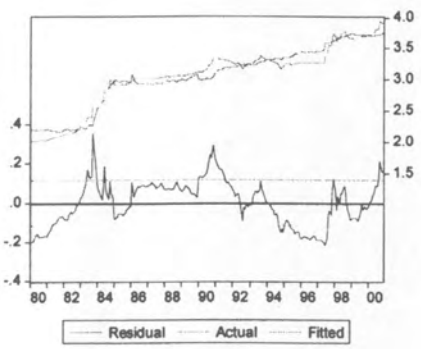

Philippine

Fig. 1: Deviations of exchange rates from linear (OLS) PPP equilibrium

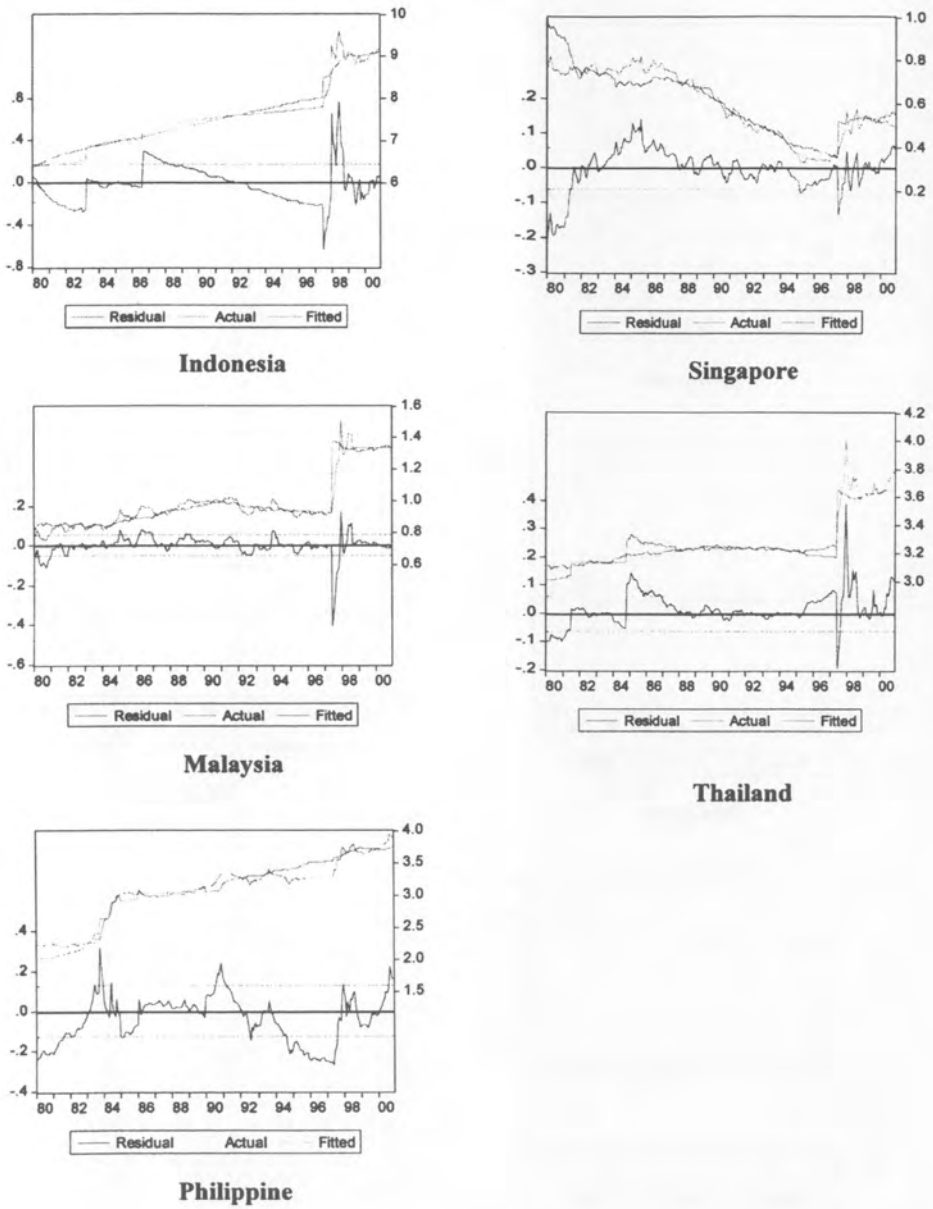

Fig. 2: Deviations of exchange rates from nonlinear symmetrical (GARCH) PPP equilibrium

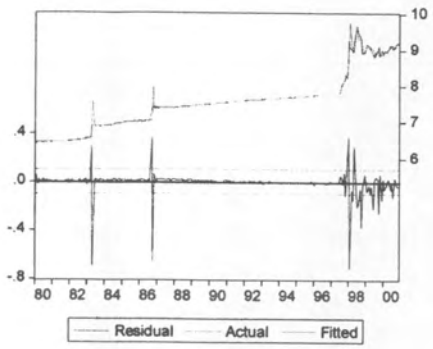

Indonesia

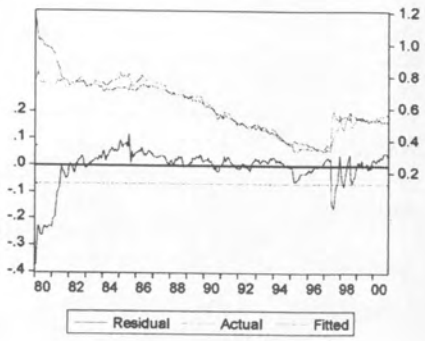

Singapore

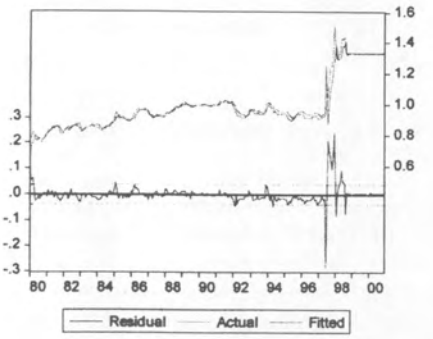

Malaysia

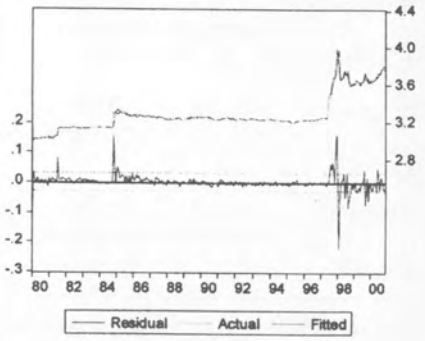

Thailand

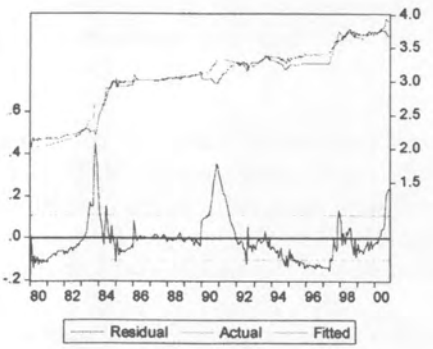

Philippine

Fig. 3: Deviations of exchange rates from nonlinear asymmetrical (EGARCH-M) PPP equilibrium

TABLE 5
Unit root tests (ADF)

	OLS		GARCH		EGARCH-M	
ASEAN 5	I	I and T	I	I and T	I	I and T
Indonesia	-3.857	-3.848	-3.848	-3.843	-21.095	-21.455
	(0.003)***	(0.016)**	(0.003)***	(0.016)**	(0.000)***	(0.000)***
Lag(SIC)	0	0	0	0	0	0
Malaysia	-4.637	-4.658	-6.284	-6.271	-4.512	-4.581
	(0.000)***	(0.001)***	(0.000)***	(0.000)***	(0.000)***	(0.001)***
Lag(SIC)	7	7	0	0	6	6
Philippine	-2.714	-2.726	-2.528	-2.523	-3.596	-3.587
	(0.073)*	(0.227)	(0.110)	(0.317)	(0.007)***	(0.033)**
Lag(SIC)	0	0	0	0	0	0
Singapore	-3.778	-3.834	-4.017	-3.978	-3.953	-3.837
	(0.004)***	(0.016)**	(0.002)***	(0.011)**	(0.002)***	(0.016)**
Lag(SIC)	0	0	0	0	0	0
Thailand	-3.740	-3.767	-3.545	-5.290	-16.97	-17.495
	(0.004)***	(0.020)**	(0.008)***	(0.000)***	(0.000)***	(0.000)***
Lag(SIC)	7	7	7	0	0	0

The optimal autoregressive terms of the ADF test are determined via Schwarz Information Criterion (SIC) with maximum lag of 12. I indicates that the ADF test includes a constant but no deterministic trend, while I and T denote the ADF with a constant and a deterministic trend. Values in the parentheses are the p-values. * denotes significance at 0.10 level ; ** denotes significance at 0.05 level and *** denotes significance at 0.01 level.

In this study, we compare the forecast of each model using the root mean square error (RMSE) and the mean absolute percentage error (MAPE). We truncate the data into two periods: the in-sample estimation period (1980: 01-2001: 02) and out-sample forecast period (2001: 03-2002: 11). Data from the in-sample period is used to estimate the parameters of the model and it includes the 1997/98b Asian financial crisis.

The encouraging findings found from the sample's good-fit and stationary test provide a tangible ground for out-of-sample forecasting. Table 6 reports the forecasting evaluation for both within sample and out-of-sample forecasting for all three models involved. Obviously, for within-sample forecasting, the RMSE criterion suggests that the linear PPP fits well as compared with the nonlinear PPP. MAPE in contrast holds up to the nonlinear PPP; where the asymmetrical EGARCH-M model provides the least MAPE for both the Philippine peso and Singapore dollar; and the symmetrical GARCH PPP model best forecasts the Malaysian ringgit. Both the RMSE and MAPE criteria however, show consistency in out-of-sample forecasting. The nonlinear PPP models show superiority in

TABLE 6
Comparison on forecasting performance of PPP models

		Within-Sample		Out-of-Sample	
ASEAN 5	Model	RMSE	MAPE	RMSE	MAPE
Indonesia	OLS	0.1716*	1.7038*	0.1472	1.3251
	GARCH	0.1746	1.7131	0.1264*	1.1631*
	EGARCH-M	0.4332	3.6766	0.9277	8.5423
Malaysia	OLS	0.0487*	3.0910	-	-
	GARCH	0.0498	2.8936*	-	-
	EGARCH-M	0.0975	7.6755	-	-
Philippine	OLS	0.1140*	3.2939	0.1791*	4.5065*
	GARCH	0.1234	3.3772	0.1857	4.6754
	EGARCH-M	0.1204	3.2865*	0.2055	5.1786
Singapore	OLS	0.0580*	7.1546	0.0860	14.3133
	GARCH	0.0587	6.7709	0.0844	14.0441
	EGARCH-M	0.0640	6.6623*	0.0772*	12.7781*
Thailand	OLS	0.0538*	1.1320*	0.0641	1.4796
	GARCH	0.0596	1.1352	0.1133	2.8795
	EGARCH-M	0.0958	2.1199	0.0507*	1.1085*

* denotes the smallest value of the RMSE and MAPE among the three models involved. The Malaysian ringgit has been pegged to USD since September 1, 1998. Hence, we exclude Malaysia from the out-of-sample forecasting comparison.

forecasting the Indonesian rupiah, Singapore dollar and Thai baht; where the GARCH model best fits the Indonesian rupiah, while EGARCH-M model best fits the Singapore dollar and Thai baht.

CONCLUDING REMARKS

This paper presents additional evidence on the dynamics of real exchange rates of the five largest ASEAN countries-Malaysia, Singapore, Thailand, Indonesia and the Philippines-for the years 1980 to 2002. To resolve the PPP puzzle in the emerging market economies, we based our analysis on monthly frequency data. In this paper, we also examine at the impact of the 1997 Asian financial crisis on the PPP relationship for the ASEAN-5 countries. The weight of the evidence suggests that real exchange rate for all the countries under investigation using the US dollar as the numeriare currency follows a stationary (mean reverting) process. Hence, this study provides new evidence that supports PPP hypothesis as a long-run relationship for the ASEAN-5 member countries. This finding appears to be robust as the result holds in both the linear and non-linear specifications. From the policy perspective, the evidence indicates that the ASEAN countries are returning to some form of PPP-oriented rule as a basis for

their exchange rate policies in order to maintain international competitiveness and to stabilize domestic economies. The convergence between exchange rate and inflation in the ASEAN countries is also an indication that the integration process in the region has begun. In the past two decades, these countries have opened their frontiers to both international commerce and investment.

All in all, the results indicate that the linear specification yield superior within sample forecast. In contrast, the GARCH-family of models dominated the standard linear PPP model in the out-of-sample forecasts. In what follows, we also observed that the conditional variance of all the ASEAN currencies (except for the ringgit) increase significantly in the post-1997 period. We also document the fact volatility in exchange rate for the ASEAN countries may be modeled by the GARCH-type of models. The statistical analysis reveals that the Philippines peso and the Singapore dollar were the least to be affected by the currency turmoil. Although Malaysia and Thailand have suffered huge undervaluation during the crisis, both the ringgit and baht are found to be corrected at a quicker pace relative to the other three currencies from the misalignments of the PPP rate. We also found that the volatility (exchange rate risk) has somewhat increased in the post crisis period for all except the ringgit, where it was pegged to the US dollar.

Finally, direction for future research include: extending this study to more bilateral rates vis-à-vis the US dollar (or yen); and comparing with the predictability of monetary model with that of PPP. The outcome from such studies will more effectively guide practitioners and managers findings in managing exchange rate risk.

ACKNOWLEDGMENTS

The first author is also a fellow research at Institute for Mathematical Research (INSPEM) and would like to acknowledge the financial support from the IRPA [No. 05-02-04-0532]. We are grateful for the comments and suggestions from the two anonymous referees. The usual disclaimer applies.

REFERENCES

AGGARWAL, R. and M. MOUGOUE. 1996. Cointegration among Asian currencies: Evidence of the increasing influence of the Japanese yen. *Japan and the World Economy* **8:** 291-308.

AZALI, M., M.S. HABIBULLAH and A.Z. BAHARUMSHAH. 2001. Does PPP hold between Asian and Japan economies? Evidence using panel unit root and panel cointegration. *Japan and World Economy* **13:** 35-50.

BAHARUMSHAH, A.Z. and M. ARIFF. 1997. Purchasing power parity in South East Asian countries: A cointegration approach. *Asian Economic Journal* **11:** 141-153.

BAHARUMSHAH, A.Z. 2002. The economics of exchange rates in the East Asian countries. Corporate Communication and International Relation Division, Universiti Putra Malaysia, Selangor.

BAHMANI-OSKOOEE, M. 1993. Purchasing power parity based on effective exchange rate and cointegration; 25 LDCs experience with its absolute formulation. *World Development* **21:** 1023-31.

BAILLIE, R.T. and T. BOLLERSLEV. 1991. Intra-day and inter-market volatility in foreign exchange rates. *Review of Economic Studies* **58:** 565-585.

BOLLERSLEV, T. 1986. Generalized autoregressive conditional heteroskedasticity. *Journal of Econometrics* **31:** 307-327.

BROOKS, C. 1996. Testing for non-linearity in daily sterling exchange rates. *Applied Financial Economics* **6:** 307-317.

BROOKS, C. 1997. Linear and non-linear (non-) forecastability of high-frequency exchange rates. *Journal of Forecasting* **16:** 125-145.

CAPORALE, G.M. and N. PITTIS. 1996. Modelling sterling-deutschmark exchange rate: Non-linear dependence and thick tail. *Economic Modelling* **13:** 1-14.

CHOO, W.C., S.S. FOONG and C.W. HOOY. 2001. Performance of various GARCH Models in forecasting the weekly exchange rates volatility. Paper presented at *FEP Seminar*, 1-5 October, Pahang.

ENGLE, C. 2000. Long run PPP may not hold after all. *Journal of International of Economics* **57:** 243-273.

GAN, W. 1991. On the deviation from purchasing power parity: The case of the ringgit effective exchange rates. *Applied Economics* **23:** 1461-1471.

HENTSCHEL, L. 1995. All in the family: nesting symmetric and asymmetric GARCH models. *Journal of Financial Economics* **39:** 71-104.

HSIEH, D.A. 1989. Testing for nonlinear dependence in daily foreign exchange rates. *Journal of Business* **62:** 339-368.

LIEW, K.S., A.Z. BAHARUMSHAH and E. LAU. 2002. Nonlinear adjustment to purchasing power parity: Empirical evidence from Asian/Yen exchange rates. *Proceedings, Asia Pacific Economics and Business Conference.* 902-910.

LIEW, K.S, A.Z. BAHARUMSHAH and T.T.L. CHONG. 2004. Are real exchange rates stationary? *Economic Letters* **83(3):** 313-316.

LIM, K.P., M. AZALI, M.S. HABIBULLAH and M.A. AZIZ. 2002. Non-linear dependence in ASEAN-5 foreign exchange markets. *Proceedings, Asia Pacific Economics and Business Conference.* 893-901.

MACDONALD, R. and M.P. TAYLOR. 1992. Exchange rate economics: A survey. *IMF Staff Paper* **39:** 1-57.

MACDONALD, R. 1997. What determines real exchange rates; The long and short run of it? International Monetary Fund Working Paper WP/97/21, International Monetary Fund, Washington D.C.

MEESE, R.A. and K. ROGOFF. 1983. Empirical exchange rates models of the seventies: Do they fit out of sample? *Journal of International Economics* **14:** 3-74.

PAPELL, D. H. 2002. The great appreciation, the great depreciation, and the purchasing power parity hypothesis. *Journal of International Economics* **57:** 51-82.

ROGOFF, K. 1996. The purchasing power parity puzzle. *Journal of Economic Literature* **34:** 647-668.

SARNO, L. 2000a. Real exchange rate behavior in high inflation countries: empirical evidence from Turkey: 1980-1997. *Applied Economic Letters* **7:** 285-291.

SARNO, L. 2000b. Real exchange rate behavior in the Middle East: a re-examination. *Economic Letters* **66:** 127-136.

SAZANAMI, Y. and S. YOSHIMURA. 1999. Restructuring East Asian exchange rate regimes. *Journal of Asian Economics* **10:** 509-523.

TARO, E. 2002. Panel unit root tests of purchasing power parity between Japanese cities, 1960-1998: disaggregated price data. *Japan and World Economy*: 1-12. (in press)

TAYLOR, M.P. 1995. The economics of exchange rates. *Journal of Economic Literature* **33:** 13-47.

VILASUSO, J. 2002. Forecasting exchange rate volatility. *Economic Letters* **76:** 59-64.

Pertanika J. Sci. & Technol. 14(1 & 2): 33 - 40 (2006)
ISSN: 0128-7680

Thermal Wave Resonant Cavity Technique in Measuring Thermal Diffusivity of Sucrose Solution

Azmi, B.Z., Sing, L.T., Saion, E.B. & Wahab, Z.A.
Department of Physics, Faculty of Science, Universiti Putra Malaysia, 43400 UPM Serdang, Selangor, Malaysia

Received: 11 December 2003

ABSTRAK

Teknik 'rongga resonan gelombang terma' telah digunakan untuk mengukur keresapan terma bagi larutan sukrosa dengan kepersisan tinggi sehingga tiga angka bererti. Keresapan terma dari larutan adalah menurun dengan peningkatan peratusan berat sukrosa dan bersetuju dengan peraturan campuran mudah dalam renj sehingga ke suatu takat tepu. Juga keresapan terma larutan berubah secara linear terhadap kuasa dua FWHM. Nilai keresapan terma bagi air adalah amat hampir dengan nilai literatur.

ABSTRACT

The thermal-wave resonant cavity technique has been used to measure thermal diffusivity of sucrose solution with precision up to three-significant-figure. The thermal diffusivity of the solution decreases linearly with the increase of sucrose weight percentage and agrees to the simple mixture rule in the range up to a saturated point. Also the solution thermal diffusivity varies linearly with square FWHM. The thermal diffusivity value of water is very close to the literature value.

Keywords: PVDF, photothermal

INTRODUCTION

Recent developments in monitoring and measuring the thermal properties of liquids by using photothermal techniques have attracted much attention. One of the technique is thermal-wave resonant cavity (TWRC) and has been applied successfully to acetone in water to determine thermal effusivity (Balderas-Lopez *et al.* 2000), to various liquids to determine thermal diffusivity (Balderas-Lopez *et al.* 2001), specific heat capacity and thermal conductivity (Caerels *et al.* 1998), to air and gas to measure thermodynamic equation of state (Pan and Mandelis, 1998), thermal diffusivity (Wang and Mandelis 1999), absolute infrared emissivity (Shen and Mandelis 1995; Shen *et al.* 1998) and monitor hydrocarbon vapours (Lima and Marin 2000).

The photothermal detector used in TWRC technique is a thin pyroelectric (PE) transducer such as polyvinylidene diflouride (PVDF) film that has strong PE effect (Kawai 1969; Bergman *et al.* 1971; Mandelis and Zver 1985; Xiao and Lang 1989; Mandelis *et al.* 1993) to detect the modulated or pulsed temperature rise induced in the material. The technique uses a modulated optical source that is a common feature of all photothermal techniques to generate thermal waves. The length and propagation characteristics of a thermal wave are simply

controlled by the frequency of the light source modulator. The spatial behaviour of the thermal wave in TWRC technique is monitored by varying the cavity length at one modulation frequency.

In this paper the TWRC technique application in monitoring the thermal diffusivity of sucrose solution is described as the saturated sucrose solution is diluted to low concentration at room temperature.

THEORY AND METHOD

The development of a photopyroelectric (PPE) detector with a various sample-to-source distance has successfully introduced the variability of the thermal-wave cavity length at single modulation frequency as another equally powerful control parameter. In order to analyse quantitatively PE quadrature data from the materials which are very weak sources of thermal waves, a general one dimensional treatment which takes into account all the energy pathways and determines explicitly the dependences of the PE signal on each and all system parameters (Mandelis *et al.* 1993). The one-dimensional theoretical geometry is shown in *Fig. 1.* When intensity modulated of light is illuminated onto a metal foil a thermal wave will be generated and then propagates to a medium next to it. By placing a PE sensor physically in contact with the medium the PE voltage will be detected. At a fixed thermal-wave oscillation frequency, $f = \omega / 2\pi$, the PE voltage signal across the detector is given by (Balderas-Lopez *et al.* 2000; Shen and Mandelis 1995).

$$V(L,\alpha_1,\omega) = Const(\omega)\frac{e^{-\sigma_1 L}}{1-\gamma_{ls}\gamma_{lp}e^{-2\sigma_l L}} \tag{1}$$

where ω is the angular frequency of light chopper, L is the cavity length, and σ_1 is the complex thermal diffusion coefficient, defined by

$$\sigma_l = (1+i)\sqrt{\frac{\omega}{2\alpha_l}} \tag{2}$$

α_l is the thermal diffusivity of the liquid sample. The interfacial thermal coefficients γ_{jk} are defined as

$$\gamma_{jk} = \frac{(1-b_{jk})}{(1+b_{jk})} \tag{3}$$

where $b_{jk} = e_j / e_k$ is the thermal coupling coefficient, the ratio of thermal effusivities of media j and k, the subscripts s, p, and l refer to the thermal-wave source, the PE material and the liquid sample, respectively.

The magnitude of the complex expression given in Eqn.(1) can be written as

$$| V(L,\alpha_p,\omega)| = Const\ (\omega)\ e^{-A_l L}, \tag{4}$$

and $$A_l = \left(\frac{\pi f}{\alpha_l}\right)^{1/2}. \tag{5}$$

where f is the light chopping frequency.

The plot of the in-phase signal versus cavity length from Eqn.(4) is a curve that has a deep valley of depth IP_{min} followed by a small peak of height IP_{max}. From this, a 'full width at half maximum' (FWHM) is defined as the width of the curve in unit length at half maximum of the in-phase signal. The half maximum signal here is the half maximum of the curve height or $\frac{1}{2}(IP_{max} + IP_{min})$.

The TWRC cell was constructed by using a thin copper foil attached to one end of a glass tube and the intensity modulated laser beam was illuminated on the foil to induce thermal wave, *Fig. 1.* Since the foil is in direct contact with the liquid sample, the thermal wave generated propagates across the liquid to reach the PVDF film PE sensor. The tube is attached to a micropositioner to alter the foil position thus altering the cavity length, L. The small PE voltage signal was fed into a pre-amplifier for signal amplification and then into a lock-in amplifier for signal analysis. The cavity length was increased by 20-micron step, and at each step the lock-in magnitude and phase signals were recorded. By plotting ln(signal) versus cavity length L, the thermal diffusivity can be obtained from the plot gradient A_l using Eqn.(5). Also by plotting in-phase signal versus L the FWHM can be obtained for the particular liquid sample.

In the following this technique is used to test a 'simple mixture rule' on thermal diffusivity in liquid media mixture. For a mixture containing x w% of medium A of thermal diffusivity α_A and $(1 - x)$ w% of medium B of thermal diffusivity then the mixture thermal diffusivity of the media α_B can be written as

$$\alpha' = \frac{(\alpha_A - \alpha_B)}{100} x + \alpha_B \tag{6}$$

RESULTS AND DISCUSSION

A saturated sucrose solution at room temperature (about 23°C) was prepared by desolving 10.5 g sucrose in 10.0 ml distilled water, i.e. the sucrose weight percentage in water is about 51.2w%. The other lower w%'s sucrose solution were made by adding proportionate weight of water in the saturated solution. In the experiment the light chopping frequency was set at 7.60Hz and care has

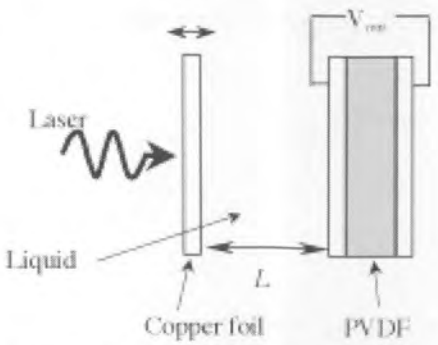

Fig. 1: Schematic diagram of thermak-wave resonant cavity cell

been taken to ensure no stray light off the glass tube hitting the PE sensor as this will introduce unwanted noise produced by the sensor.

From 9 data sets of 8 sucrose solutions of various w%'s and one of distilled water, the overal variation of PE voltage signal versus cavity length L is displayed in a 3-D spline surface plot in *Fig. 2.* The signal decreases exponentialy with cavity length for all w%'s but with different exponential constants. Here, the plain distilled water produces the highest PE signal of all sucrose solutions.

From Eqn.(4), the thermal diffusivity is obtained by plotting ln(signal) versus cavity length and for a particular case of 6.4w% sucrose solution is as can be seen in *Fig. 3.* The plot gradient is an exponential constant and the plot

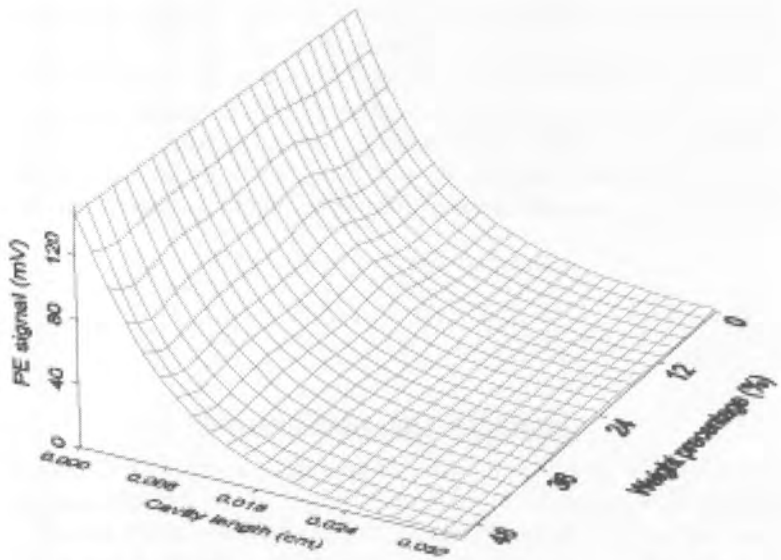

Fig. 2: Plot of PE voltage versus cavity length at various sucrose w%

is linear fitted by using Microsoft Origin software. The gradient and the thermal diffusivity are 130.860cm^{-1} and 0.139 10^{-2} cm^2/s, respectively. Here, the gradient is obtained by fitting only the first 15 data points that contribute to the good fit because at very large L they deviate from the line as the noise dominates. The pre-amplifier gain was set at 100 and the data points from the lock-in amplifier were read in millivolt. The thermal diffusivity error is mainly due to the gradient and is about 4%.

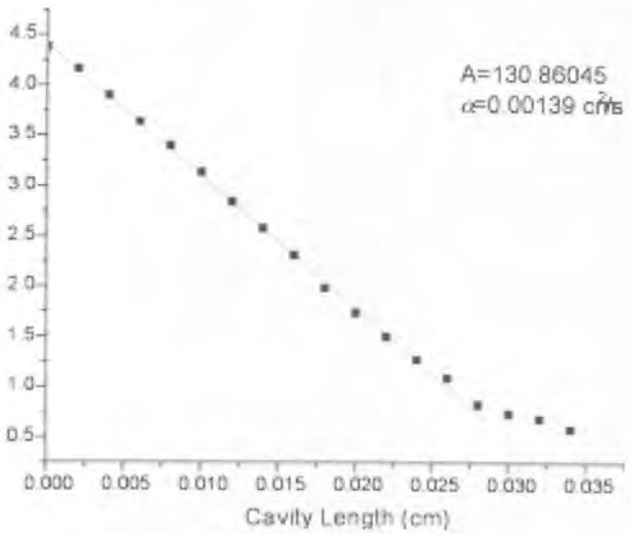

Fig. 3: ln(PE signal) versus cavity length for 6.4w% of sucrose in water

The FWHM was obtained by fitting the inphase signal by using the value obtained from the experiment. This is because the magnitude and phase data obtained were limited up to certain value of L immediately after the minimum valley before the noise starts to dominates at large L. The fitting constant was then used to extrapolate the curve slightly beyond the small peak that is not actually covered by the experimental data points (*Fig. 4*). This is acceptable because it is merely extending the data points by fitting the existing experimental data so that the FWHM of the curve can be determined.

The plot of sucrose solution thermal diffusivity α' versus w% sucrose, *Fig. 5*, shows that α' decreases linearly with w% starting from the value for the plain water or for 0w% sucrose. This corresponds very well with the simple mixture rule of Eqn.(6) for sucrose solution up to about 51.2w%. From the plot, the water thermal diffusivity obtained from the intersection of the fitted line to the verticle axis is 0.144×10^{-2} cm^2/s, that is similar to the one obtained by Balderas-Lopez *et al.* (2000) by using the technique. From this linear relationship, the thermal diffusivity of the saturated solution (51.2w% sucrose) is 0.102×10^{-2} cm^2/s. It is accepted that, for liquids, the thermal diffusivity decreases with

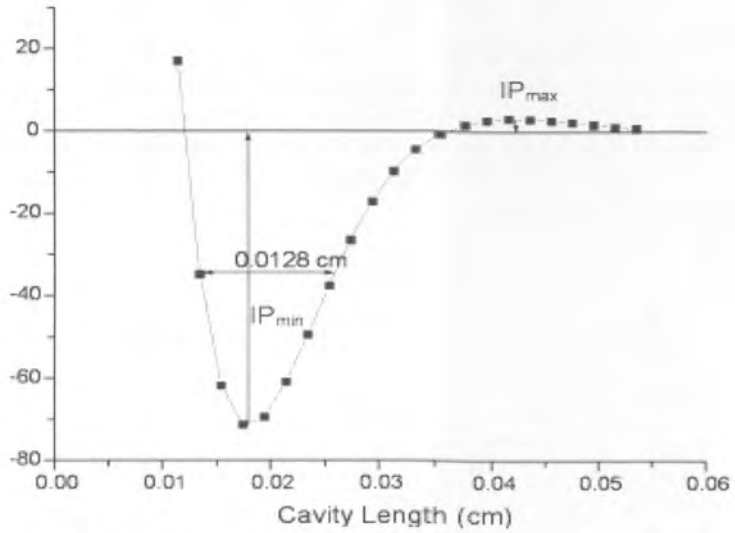

Fig. 4: In-phase signal versus cavity length at 6.4w% of sucrose in water

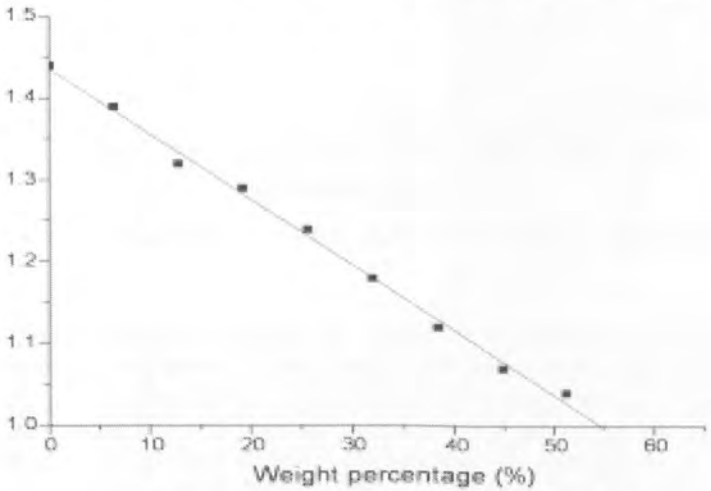

Fig. 5: Plot of thermal diffusivity versus sucrose w%

increasing molecular size. Here, the sucrose molecule is bigger in dimension compared to water, hence increasing the sucrose w% decreases the thermal diffusivity of the solution. For the very high concentration value, i.e. higher than 51.2w%, the thermal diffusivity would be constant and has the value of that of 51.2w% because the undilluted sucrose crystal settles at the bottom of the cavity instead of suspended homogenously in the solution.

The plot of mixture thermal diffusivity α' of sucrose solution versus $(FWHM)^2$, *Fig. 6*, shows that α' increases linearly with $(FWHM)^2$. This indicates that the relationship of α' and FWHM can takes the following form;

$$\alpha' = M \times (FWHM)^2 + N,$$

where M is the gradient ($8.099 \pm 0.527\ s^{-1}$) and N is the intersection with verticle axis α' ($0.092 \times 10^{-3} \pm 0.075 \times 10^{-3}\ cm.s^{-1}$). A few scattered points are due to erors in determining FWHM of a particular w% sucrose. This implies that FWHM can be a sensitive indicator to liquid thermal diffusivitiy changes.

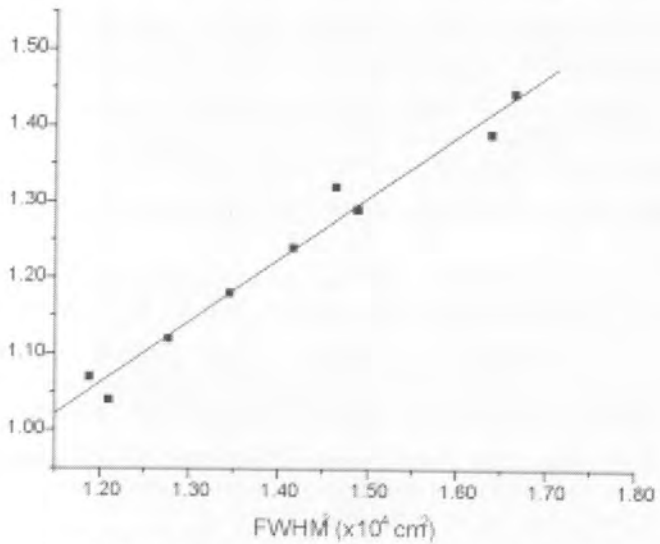

Fig. 6: Liquid mixture thermal diffusivity versus (FWHM)²

CONCLUSION

Thermal diffusivity values for sucrose solution up to saturated solution can be expressed using a simple mixture rule. The thermal diffusivity value of water is very close to the literature value. The square of FWHM varies linearly with thermal diffusivity of sucrose solution up to sucrose saturated solution.

ACKNOWLEDGEMENT

The authors are grateful to the Ministry of Science, Technology and the Environment of Malaysia for supporting this work under IRPA Grant No. 02-02-04-0132-EA001.

REFERENCES

BALDERAS-LOPEZ, J. A., A. MANDELIS and J. A. GARCIA. 2000. Thermal-wave resonator cavity design and measurements of the thermal diffusivity of liquids. *Rev. Sci. Instrum.* **71(7):** 2933-2937.

BALDERAS-LOPEZ, J. A., A. MANDELIS and J. A. GARCIA. 2001. Measurements of the thermal diffusivity of liquids with a thermal-wave resonator cavity. *Analytical Sciences* **17**: s519-522.

BERGMAN, J. B., J. H. MCFEE and G. R. CRANE. 1971. Pyroelectricity and optical second harmonic generation in polyvinylidene fluoride films. *Appl. Phys. Lett.* **18**: 203-205.

CAERELS, J., C. GLORIEUX and J. THOEN. 1998. Absolute values of specific heat capacity and thermal conductivity of liquids from different modes of operation of a simple photopyroelectric setup. *Rev. Sci. Instrum.* **69(6):** 2452-2458.

KAWAI, H. 1969. The piezoelectricity of poly (vinylidene fluoride). *J. Appl. Phys.* **8:** 975-976.

LIMA, J. A. P. and E. MARIN. 2000. On the use of the thermal wave resonator cavity sensor for monitoring hydrocarbon vapors. *Rev. Sci. Instrum.* **71(7):** 2928-2932.

MANDELIS, A., J. VANNIASINKAM and S. BUDHUDU. 1993. Absolute nonradiative energy-conversion-efficiency spectra in Ti^{3+}: Al_2O_3 crystal measured by noncantact quadrature photopyroelectric spectroscopy. *Physical Review B* **48(10):** 6808-6821.

PAN, G. and A. MANDELIS. 1998. Measurement of the thermodynamic equation of state via the pressure dependence of thermophysical properties of air by a thermal-wave resonant cavity. *Rev. Sci. Instrum.* **69(8):** 2918-2923.

SHEN, J. and A. MANDELIS. 1995. Thermal-wave resonator cavity. *Rev. Sci. Instrum.* **66(10):** 4999-5005.

SHEN, J., A. MANDELIS and H. TSAI. 1998. Signal generation mechanism, intracavity-gas thermal-diffusivity temperature dependence, and absolute infrared emissivity measuarements of thermal-wave resonant cavity. *Rev. Sci. Instrum.* **69(1):** 197-203.

WANG, C. and A. MANDELIS. 1999. Measurement of thermal diffusivity of air using photopyroelectric interferometry. *Rev. Sci. Instrum.* **70(5):** 2372-2378.

XIAO, D. Q. and S. B. LANG. 1989. Measurement applications based on PE properties of ferroelectric's polymers. *IEEE Trans. Electr. Insul.* **23:** 503-516.

Pertanika J. Sci. & Technol. 14(1 & 2): 41 - 52 (2006)
ISSN: 0128-7680

Kajian Mengenai Kebersandaran Pembentukan Keadaan Potong Bawah Penjuru Terhadap Jenis Larutan Pemunar dalam Penghasilan Diafram Beralun Silikon

[1]Norhayati Soin & [2]Burhanuddin Yeop Majlis
[1]Jabatan Kejuruteraan Elektrik
Fakulti Kejuruteraan, Universiti Malaya
50603 Kuala Lumpur, Malaysia
Email: norhayatisoin@um.edu.my
[2]Institut Kejuruteraan Mikro dan Nanoelektronik (IMEN)
Universiti Kebangsaan Malaysia
43600 UKM, Bangi, Selangor, Malaysia

Received: 18 August 2005

ABSTRAK

Kertas kerja ini membentangkan hasil kajian simulasi mengenai kesan jenis larutan pemunar ke atas keadaan potong bawah penjuru yang terhasil pada struktur-struktur penjuru cembung diafram beralun silikon (100). Diafram yang terlibat dalam kajian ini dihasilkan dengan menggunakan teknik punaran anisotropik dengan larutan kalium hidroksida (KOH) dan larutan tetrametil amonia hidroksida (TMAH) sebagai pemunar. Kerja-kerja simulasi telah dijalankan dengan menggunakan perisian proses punaran anisotropik Intellisuite. Berdasarkan geometri struktur penjuru cembung terpunar dan kemunculan satah-satah baru silikon, diafram beralun silikon yang dipunarkan di dalam larutan TMAH didapati mengalami keadaan potong bawah penjuru yang lebih ketara berbanding diafram yang dipunarkan dalam larutan KOH.

ABSTRACT

This paper describes the simulation study of the effect of the etchant type on the convex corner phenomenon of the silicon (100) corrugated diaphragm during the anisotropic etching process. Potassium hydroxide (KOH) and tetramethyl ammonium hydroxide (TMAH) were used as an etchant in order to produce the diaphragm respectively. The Intellisuite process simulation software has been used in this simulation. Based on the geometrical etched structure of the convex corners and the emergent of the new silicon planes, the convex corner-undercutting phenomenon was found to be much more pronounced when TMAH is used as the etchant.

Kata kunci: Diafram beralun, punaran anisotropik, satah baru silikon, potong bawah penjuru

PENGENALAN

Pada masa ini pembangunan yang penting telah dihasilkan dalam membina struktur-struktur sistem mikro elektro mekanikal (MEMS) dengan menggunakan teknologi-teknologi yang berasal dari fabrikasi litar bersepadu. Fabrikasi struktur-

struktur kecil MEMS ini memerlukan pemesinan mikro yang amat tepat. Dalam kes ini, proses punaran basah anisotropik telah dikenal pasti sebagai salah satu proses yang merupakan asas kepada fabrikasi struktur-struktur MEMS dan terdapat banyak kajian yang telah dibuat secara eksperimen dan teori untuk memahami mekanisme proses punaran ini (Shikida *et al.* 2001). Seidel *et al.* (1990) dan Glembocki *et al.* (1991) telah menghasilkan model-model bagi proses punaran ini dan mengkaji mengenai ciri-ciri punaran ini di bawah pelbagai keadaan punaran.

Proses punaran basah ini melibatkan silikon berhablur tunggal yang dipunarkan secara kimia dengan menggunakan larutan pemunar. Sehingga kini larutan alkali berair termasuk larutan berair organik tetrametil amonia hidroksida (TMAH) (Shikida *et al.* 2001; Merlos *et al.* 1993), ethylenediamine-pyrocatechol (EDP), atau hydrazine- pyrocatechol dan larutan-larutan berair inorganik seperti potassium hidroksida (KOH) dan ammonium hidroksida (NH_4OH) telah digunakan sebagai larutan pemunar (Glembocki *et al.* 1991). Larutan pemunar yang paling popular di antara larutan-larutan pemunar tersebut adalah larutan yang berasaskan KOH. Larutan pemunar yang berasaskan KOH ini mempunyai ciri-ciri seperti darjah keberacunan yang rendah dan bersifat ketakmudahbakaran yang menyebabkan kos proses fabrikasi yang rendah, pengelolaan yang mudah dan pencemaran persekitaran yang rendah (Seidel *et al.* 1990).

Sungguhpun banyak penyelidikan mengenai proses punaran basah tersebut telah dilaporkan sebelum ini, masalah-masalah serius dalam pemahaman dan pengawalan yang melibatkan proses-proses fizik dan elektrokimia masih lagi wujud (Schroder *et al.* 1998). Masalah-masalah ini merupakan perkara yang amat penting dan perlu diberi perhatian dari aspek ekonomi bagi proses fabrikasi sesuatu peranti. Kelakuan punaran ini mestilah dipastikan akan kestabilan dan kebolehramalannya, terutamanya nisbah anisotropi (dalam punaran dibahagikan dengan jumlah penjuru terpunar (Seidel *et al.* 1990)) yang sepatutnya mempunyai kebolehkeluaran semula dengan kejituan yang tinggi dan permukaan-permukaan terpunar yang licin.

Dalam kajian-kajian sebelum ini, suatu perbandingan maklumat-maklumat mengenai proses punaran yang dihasilkan telah menunjukkan dengan jelasnya akan kewujudan masalah-masalah tersebut (Seidel *et al.* 1990; Tellier dan Durand 1997; Kendall 1990; Zavracky 1997). Struktur bentuk yang dihasilkan dari punaran anisotropik tidak hanya bergantung pada orientasi hablur, kepekatan KOH, suhu punaran, kepekatan dopan boron, jenis larutan pemunar (Seidel *et al.* 1990) tetapi juga kepada bentuk dan penjajaran topeng punaran (Glembocki *et al.* 1991).

Kebiasaannya struktur-struktur yang dibentuk dengan menggunakan punaran anisotropik ini terdiri daripada penjuru cembung seperti yang terdapat dalam sensor tekanan dan mikro pam (Li *et al.* 2000). Struktur-struktur tersebut adalah seperti diafram-diafram bertombol, alur-alur berbentuk V dan lain-lain struktur yang melibatkan penjuru cembong yang selalu mengalami keadaan penjuru terpunar dan memerlukan topeng-topeng yang direka bentuk dengan

struktur-struktur tambahan pampasan penjuru. Keadaan potong bawah penjuru ini merupakan kesan yang tidak dikehendaki dalam pemesinan mikro silikon seperti dalam fabrikasi sensor-sensor mekanikal dengan penjuru cembong yang sempurna adalah penting bagi spesifikasi peranti yang baik.

Objektif kertas kerja ini adalah untuk membuat kajian secara simulasi mengenai pengaruh jenis larutan pemunar ke atas pembentukan keadaan potong bawah penjuru yang terhasil pada diafram beralun silikon. Ini meliputi kerja-kerja pencirian struktur–struktur penjuru cembung yang terpunar secara geometri dan pengenalpastian satah-satah silikon baru yang muncul pada permukaan terpunar tersebut.

PERISIAN SIMULASI PUNARAN ANISOTROPIK INTELLISUITE

Dalam kertas ini kajian simulasi dijalankan dengan menggunakan perisian reka bentuk berbantu komputer (CAD) IntelliSense Software Versi 7.1 yang dibangunkan oleh Intellisuite Corporation (Finch *et al.* 2004). Perisian ini mampu menyediakan kemudahan simulasi yang mempunyai ketepatan yang tinggi untuk peranti-peranti MEMS daripada kategori-kategori yang berlainan prinsip operasinya (mekanik, elektrostatik dan elektromagnetik) dan seterusnya menghasilkan kemunculan gambaran secara grafik untuk peranti yang telah melalui proses punaran secara simulasi (Marchetti *et al.* 1998).

Perisian ini merupakan suatu perisian bersepadu yang kompleks yang boleh membantu pereka-pereka bentuk mengoptimumkan peranti-peranti MEMS dengan memberikan mereka capaian kepada pengkalan data pengilangan dan dengan membenarkan mereka untuk memodelkan keseluruhan turutan pengilangan suatu peranti serta seterusnya mensimulasi ciri-ciri untuk mendapatkan hasil simulasi secara visual tanpa menggunakan kemudahan pengilangan yang sebenar (Marchetti *et al.* 1998).

STRUKTUR DIAFRAM

Struktur diafram yang terlibat dalam kajian ini adalah seperti yang ditunjukkan dalam *Rajah 1.* Diafram tersebut adalah berbentuk segi empat dan bersaiz 7.2 mm x 7.2 mm serta mempunyai corak alunan berbentuk segi empat sepusat. Jumlah alunan yang terdapat di atas diafram tersebut adalah sebanyak tiga. Struktur-struktur alunan tersebut akan direalisasikan dengan menggunakan teknik punaran anisotropik. Parameter-parameter struktur diafram beralun tersebut adalah seperti yang disenaraikan dalam Jadual 1. Reka bentuk topeng punaran yang akan digunakan dalam proses punaran bagi pembentukan struktur diafram beralun ini adalah seperti yang ditunjukkan dalam *Rajah 2.*

ANALISIS CIRI-CIRI KEADAAN POTONG BAWAH PENJURU

Bahagian ini membincangkan mengenai ciri-ciri keadaan potong bawah penjuru yang terbentuk pada penjuru cembung reka bentuk diafram beralun yang diperoleh daripada kerja-kerja simulasi. Pencirian keadaan potong bawah penjuru

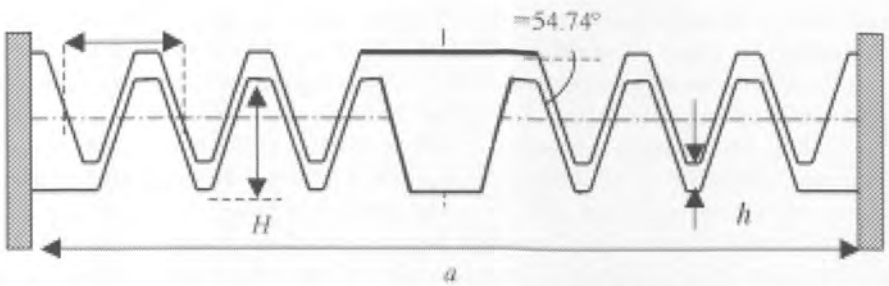

Rajah 1: Pandangan keratan rentas diafram beralun silikon

JADUAL 1
Parameter-parameter bagi struktur diafram beralun silikon

Parameter	Simbol	Nilai
Panjang sisi	a	7.2 mm
Tebal diafram	h	284 μm
Dalam alunan	H	216 μm
Jarak gelombang	,	584 μm
Sudut di antara satah (100) dan dinding tepi	θ	54.74°

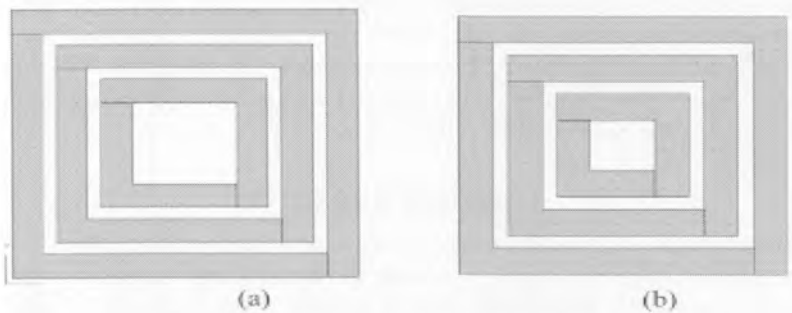

Rajah 2: Bentangan topeng bagi struktur diafram beralun silikon bahagian (a) atas dan (b) bawah

tersebut termasuklah mengenal pasti kemunculan satah-satah silikon yang baru pada penjuru cembung semasa proses punaran, jumlah keadaan potong bawah penjuru yang berlaku pada arah 45° kepada satah permukaan rata (100) dan arah <110>.

Keputusan kajian ini adalah seperti yang ditunjukkan dalam *Rajah 3* dan *4*. Memandangkan simulasi proses punaran ini telah dilakukan pada kedua-dua bahagian wafer silikon tanpa menggunakan bentangan topeng pampasan, kelihatan terdapat lubang-lubang yang terhasil pada kesemua penjuru cembung

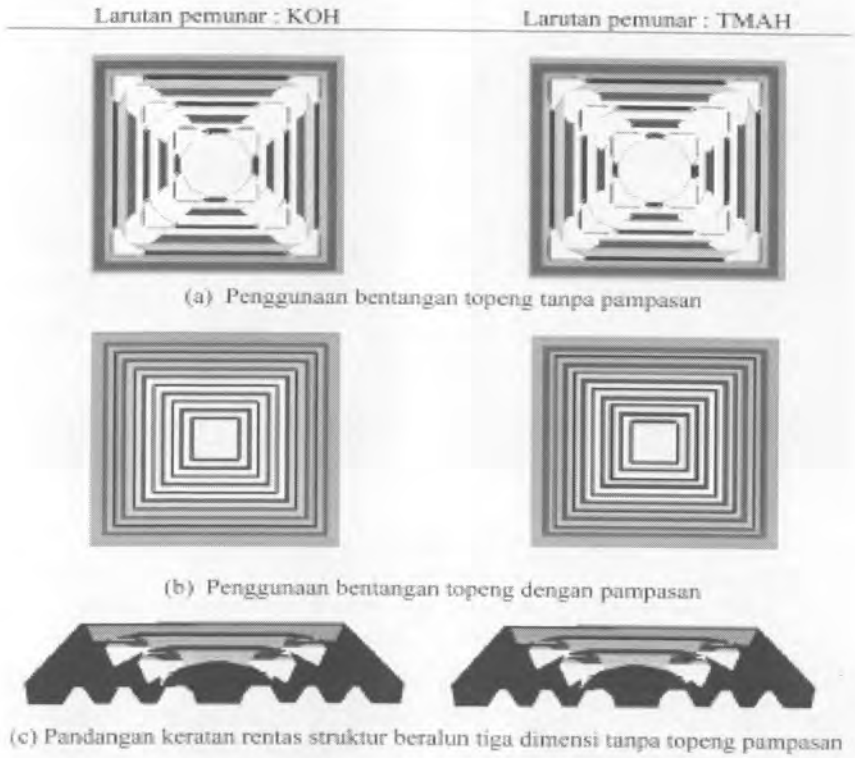

Rajah 3: Hasil-hasil simulasi dengan perisian AnisE untuk diafram beralun silikon

diafram beralun. Bagi memudahkan kerja-kerja pencirian keadaan potong bawah penjuru, hanya bahagian atas diafram beralun telah dipertimbangkan untuk tujuan analisis. Ini adalah disebabkan oleh persamaan struktur-struktur alunan yang telah direka bentuk pada kedua-dua bahagian diafram itu secara geometri. Tambahan pula jika kedua-dua bahagian atas dan bawah dipertimbangkan untuk proses punaran, pencirian keadaan potong bawah penjuru tidak boleh dilakukan kerana wujudnya lubang-lubang pada setiap struktur penjuru cembung hasil daripada proses punaran dari arah atas dan bawah diafram. Daripada keputusan ini, jika pandangan dibuat secara bersudut tepat pada bahagian atas diafram, keadaan potong bawah penjuru yang terhasil boleh disifatkan seperti yang diberikan dalam *Rajah 5* dan *6*. Diafram beralun tersebut memulakan pengubahsuaian ke atas bentuk semua penjuru cembung dengan menukarnya kepada bentuk-bentuk yang berlainan yang mempunyai satah berindeks tinggi.

Daripada *Rajah 4*, kelihatan keadaan potong bawah penjuru adalah lebih ketara pada diafram yang dipunarkan dengan menggunakan larutan TMAH berbanding dengan larutan KOH. Secara pandangan kasar, perbezaan ciri-ciri keadaan potong bawah penjuru yang didapati daripada hasil simulasi tersebut

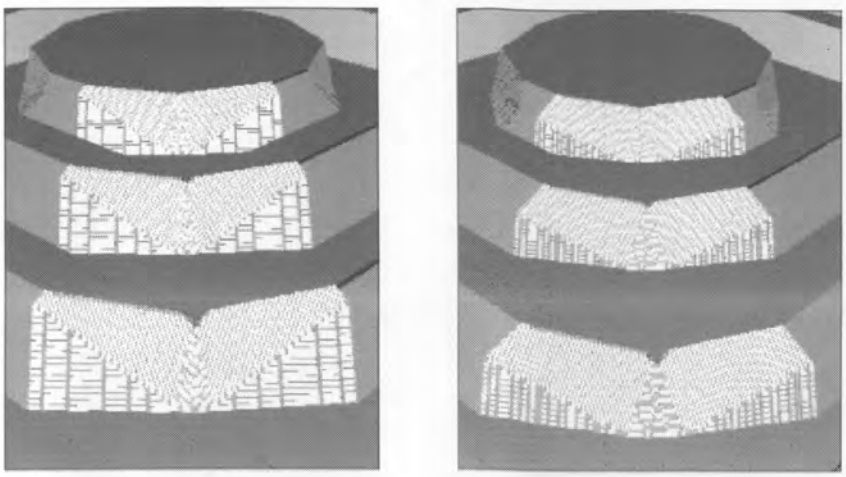

(a) (b)

Rajah 4: Pandangan secara dekat kesan jenis larutan pemunar: (a) KOH dan (b) TMAH terhadap ciri-ciri keadaan penjuru terpunar pada beberapa bahagian struktur penjuru cembung pada diafram beralun

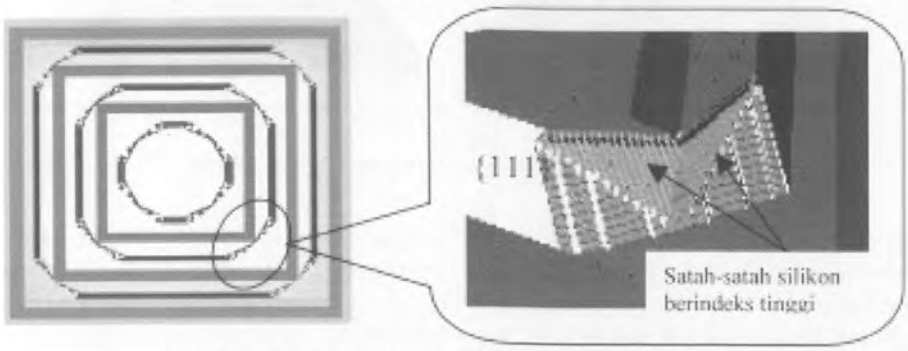

Rajah 5: Hasil simulasi pandangan atas dan fenomena potong bawah penjuru pada diafram beralun

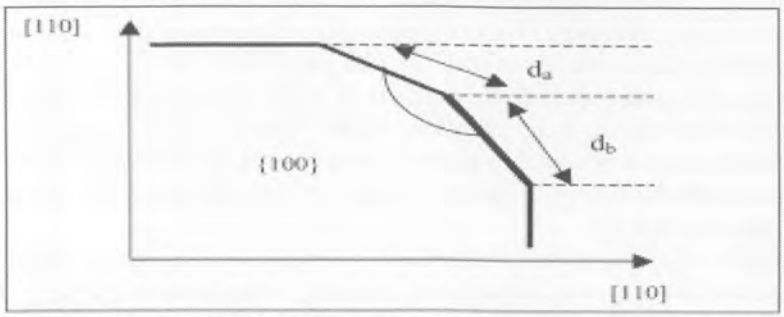

Rajah 6: Pandangan atas dua dimensi suatu penjuru cembung yang terpunar dengan takrifan sudut terhasil, α dan jarak-jarak d_a dan d_b

lebih ketara berlaku pada sudut, κ di antara satah yang baru muncul dan bahagian bawah wafer silikon dengan nilai sudut ini adalah lebih kecil dalam kes larutan pemunar TMAH (rujuk kepada *Rajah 7*). Oleh itu, kawasan bahagian atas penjuru cembung yang telah terpunar atau permukaan satah baru muncul dalam larutan TMAH adalah lebih besar berbanding dengan hasil penjuru cembung yang terpunar dalam larutan KOH. Kenyataan ini disahkan apabila pengukuran bagi dimensi-dimensi struktur potong bawah penjuru yang terhasil dibuat dengan kemudahan perkakas pengukuran yang terdapat dalam perisian AnisE yang dihasilkan oleh Intellisuite Corporation (*http://www.intellisensesoftware*) dan seterusnya ditunjukkan seperti dalam Jadual 2. Takrifan bagi parameter-parameter yang terdapat dalam Jadual 2 boleh didapati dalam *Rajah 7.*

Daripada hasil pengukuran ini, sudut penjuru cembung yang terpunar, α, dalam larutan TMAH didapati lebih kecil daripada hasil yang didapati dari proses punaran KOH apabila rujukan dibuat kepada *Rajah 5* dengan nilai sudut penjuru cembung yang terpunar, α, yang kecil menandakan keadaan penjuru cembung yang terpunar yang lebih ketara. Bagi proses punaran KOH pula, sudut α yang telah diukur daripada kajian ini mempunyai nilai yang lebih

JADUAL 2
Pencirian keadaan potong bawah penjuru yang dihasilkan oleh larutan pemunar KOH dan TMAH

Parameter	Larutan KOH	Larutan TMAH
d_a (μm)	521.34	541.92
d_b (μm)	518.70	543.86
d_c (μm)	20.89	80.11
d_d (μm)	575.18	584.37
d_e (μm)	204.25	135.92
κ (°)	22.80	12.43
α (°)	150.21	145.80

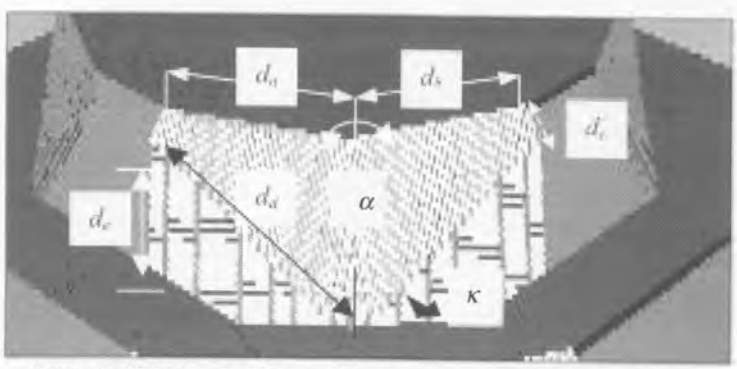

Rajah 7: Takrifan bagi parameter-parameter yang digunakan bagi pencirian potong bawah penjuru untuk rujukan Jadual 1

daripada apa yang dihasilkan oleh larutan TMAH dan nilainya hampir serupa dengan satah-satah {411} iaitu 151.20° (Runyan 1965) manakala untuk proses punaran TMAH sudut α mempunyai nilai yang kurang dari satah-satah {411}. Oleh yang demikian, diafram beralun yang dipunarkan di dalam larutan TMAH mengalami keadaan potong bawah penjuru yang lebih ketara berbanding jika ia dipunarkan dalam larutan KOH. Keputusan simulasi ini adalah bertepatan dengan kajian uji kaji yang telah dibuat mengenai proses punaran anistropik silikon di dalam larutan TMAH sebelum ini (Sonphao dan Chaisirikul 2001).

Nilai-nilai parameter yang terdapat dalam Jadual 2 adalah berdasarkan pengukuran yang dibuat ke atas empat struktur penjuru cembung yang terdapat pada bahagian tengah diafram beralun yang masing-masing menghasilkan sudut terpunar α_1, α_2, α_3 dan α_4 dan parameter-parameter d_1, d_2, d_3 dan d_4 seperti yang ditunjukkan dalam *Rajah 7* dengan kemudiannya nilai purata sahaja yang dipertimbangkan. Dalam kes ini parameter d_a dan d_b dianggap mempunyai nilai yang sama berdasarkan nilai-nilai yang terdapat dalam Jadual 2 dengan nilai puratanya sahaja akan dipertimbangkan bagi menghasilkan nilai-nilai bagi parameter d_1, d_2, d_3 dan d_4. Bagi tujuan kerja-kerja pencirian keadaan potong bawah penjuru yang seterusnya hanya nilai purata parameter-parameter d_1, d_2, d_3 dan d_4 iaitu d_{ave} dan nilai purata parameter-parameter sudut terpunar α_1, α_2, α_3 dan α_4 iaitu α_{ave} yang akan dipertimbangkan.

Disamping itu, kaedah yang lebih jelas lagi bagi menunjukkan perbezaan keadaan potong bawah penjuru yang diperolehi dari hasil punaran ke atas diafram beralun ini dengan menggunakan kedua-dua larutan punaran yang berbeza ini adalah melalui pengukuran jumlah penjuru yang terpunar dari arah 45° kepada satah permukaan rata (100), $U_{<100>}$ dan dari arah <110>, $U_{<110>}$. Pengukuran ini dilakukan berdasarkan nilai-nilai purata sudut terpotong, α_{ave}, dan panjang sisi, d_{ave}, yang diperoleh dari hasil simulasi di mana pengiraan dibuat dengan merujuk kepada *Rajah 9*. Rajah ini menunjukkan model dua dimensi suatu penjuru cembung terpunar yang dilihat dari atas di mana parameter-parameter x, y, ψ, σ dan seterusnya $U_{<100>}$ dan $U_{<110>}$ ditentukan dengan menggunakan prinsip trigonometri seperti yang ditunjukkan dalam Jadual 3.

Dengan merujuk kepada keputusan dari Jadual 3, jumlah potong bawah penjuru dalam arah <100> dan <110> bagi diafram beralun yang dipunarkan dengan menggunakan larutan TMAH didapati lebih besar berbanding dengan yang dipunarkan dengan larutan KOH. Ini mengesahkan lagi kajian uji kaji yang telah dibuat mengenai proses punaran anistropik silikon di dalam larutan TMAH sebelum ini (Sonphao *et al.* 2001).

Keadaan punaran wafer silikon {100} dengan menggunakan larutan KOH dan TMAH untuk menghasilkan diafram beralun mengikut spesifikasi yang telah diberikan adalah seperti yang telah diringkaskan dalam Jadual 4. Penentuan keadaan proses simulasi punaran KOH dibuat dengan merujuk kepada keputusan-keputusan kajian uji kaji proses punaran yang telah dijalankan di makmal Institut Kejuruteraan Mikro dan Nanoelektronik, Universiti Kebangsaan Malaysia (IMEN-UKM) (Mimiwati 2003). Kajian tersebut telah dilakukan ke atas

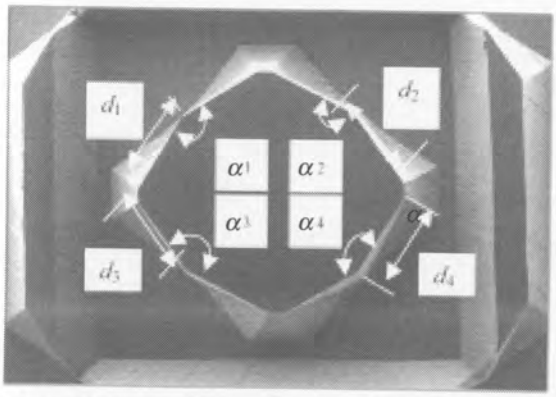

Rajah 8: Contoh-contoh struktur penjuru cembung terpunar, α_1, α_2, α_3, dan α_4 dan parameter parameter d_1, d_2, d_3 dan d_4 sebagai rujukan dalam pengukuran jumlah potong bawah penjuru

JADUAL 3
Keputusan pengiraan jumlah potong bawah penjuru dan parameter-parameter yang berkenaan dengan merujuk kepada *Rajah* 8

Jenis Pemunar	d_{ave} (μm)	α_{ave} (°)	ψ (°)	σ (°)	$U_{<100>}$ (μm)	$U_{<110>}$ (μm)
KOH	520.02	150.21	104.90	30.10	368.81	710.67
TMAH	541.89	148.8	105.6	28.90	376.20	738.11

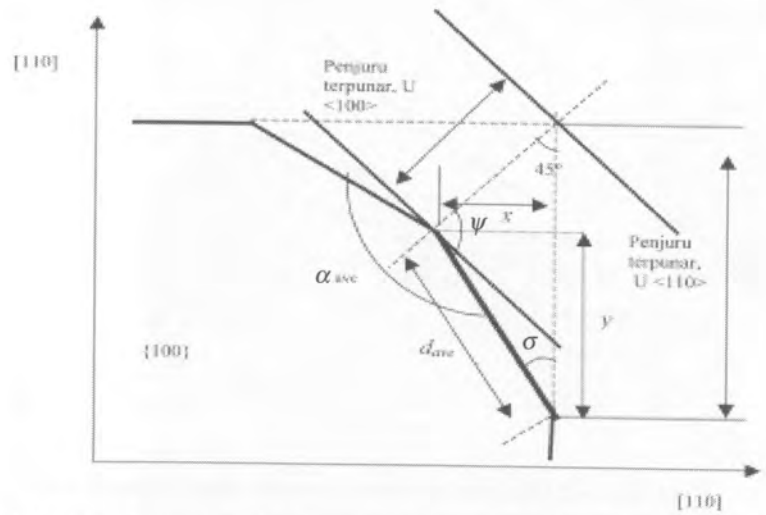

Rajah 9: Pandangan atas dua dimensi suatu penjuru cembung yang terpunar dengan takrifan sudut terhasil, α_{ave} dan parameter–parameter d_{ave}, x, y, ψ dan σ bagi rujukan penentuan jumlah penjuru cembung terpunar

JADUAL 4
Ringkasan maklumat keadaan punaran untuk proses simulasi

Parameter punaran	Larutan KOH	Larutan TMAH
Suhu (°C)	80	80
Kepekatan larutan pemunar	35%	35%
Masa punaran (jam)	3.5	7.0
Kadar punaran (μm/jam)		
Si {100}	72.55	30.13
Si {110}	111.7	53.85
Purata ketebalan diafram (μm)	38.50	38.50
Purata kedalaman alunan (μm)	$\approx$ 216	$\approx$ 216

wafer silikon jenis-n berorientasi (100) dengan menggunakan kepekatan larutan KOH yang berlainan iaitu dari 15% hingga 55%, manakala suhu punaran yang digunakan adalah bernilai dari 65°C hingga 85°C.

Keputusan kajian ini terhadap kekasaran permukaan wafer silikon yang telah dipunarkan adalah seperti yang ditunjukkan dalam *Rajah 10.* Kenaikan suhu menyebabkan kekasaran permukaan silikon meningkat sehingga kepada suatu takat maksimum iaitu 75°C untuk semua keadaan kepekatan larutan KOH. Walau bagaimanapun, pada semua keadaan kepekatan, graf dalam *Rajah 10* menunjukkan penurunan kekasaran permukaan selepas suhu 75°C.

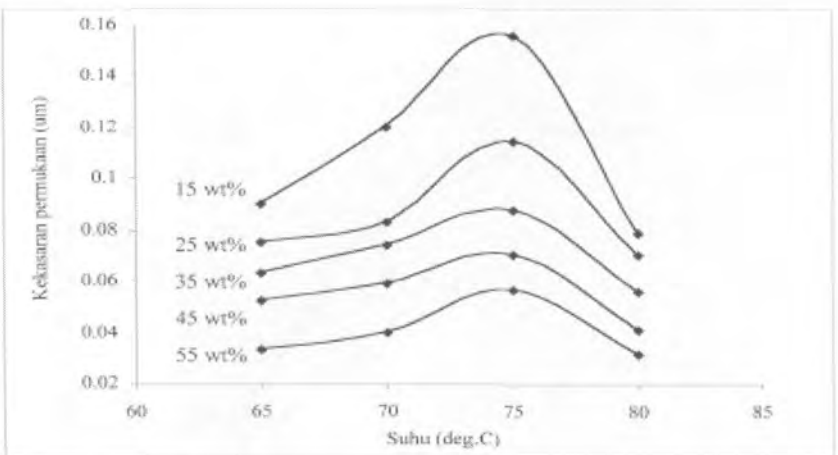

Rajah 10: Graf kekasaran permukaan diafram silikon melawan suhu pada kepekatan larutan KOH yang berlainan

KESIMPULAN

Kajian ini telah membuktikan bahawa ciri-ciri potong bawah penjuru bagi diafram beralun silikon dipengaruhi oleh jenis larutan pemunar. Kepentingan pengaruh faktor ini boleh ditentukan dengan saiz geometri struktur terpunar dan kemunculan satah-satah baru silikon pada penjuru cembung yang terpunar. Hasil dari kajian ini, permukaan penjuru cembung yang terpunar dapat disimpulkan terdiri daripada kemunculan satah-satah silikon baru yang berindeks tinggi yang berada berhampiran dengan nilai satah-satah {411} dan {511}. Oleh yang demikian pemilihan larutan pemunar yang sesuai adalah penting bagi proses penghasilan diafram beralun silikon dengan menggunakan teknik punaran anisotropik untuk mengurangkan keadaan potong bawah penjuru. Walau bagaimanapun bagi penghasilan struktur diafram yang sempurna tanpa keadaan penjuru terpotong, penggunaan topeng pampasan penjuru dan pengawalan keadaan punaran perlu dipertimbangkan. Keputusan dari kajian ini juga menunjukkan bahawa kekasaran permukaan yang tinggi atau kualiti permukaan yang kurang baik terhasil pada struktur terpunar pada keadaan punaran yang mempunyai suatu suhu yang malar dan larutan KOH yang berkepekatan rendah manakala larutan KOH yang mempunyai kepekatan yang tinggi akan menghasilkan kekasaran permukaan yang rendah atau kualiti permukaan yang sangat baik.

RUJUKAN

FINCH, N., Y. HE and J. MARCHETTI. 2004. 'General MEMS Process Physics Simulation and its Applications' IntelliSense Corporation, 36 Jonspin Road, Wilmington, MA USA.

GLEMBOCKI, O. J., E. D. PALIK, G. R DE GUEL and D. L KENDALL. 1991. Hydration model for the molarity dependence of etch rate of Si in aqueous alkali hydroxides. *J. Electrochem. Soc.* **138(4):** 1055-1063.

http://www.intellisensesoftware.com/datasheets/Intellisuite_2004.pdf

KENDALL, D. L. 1990. A new theory for the anisotropic etching of silicon and some underdeveloped chemical micromachining concepts. *Vac. Sci. Technol.* A **8(4):** 3598-3605.

LI, X., L. RONGMING, M. JIANMIN and M. BAO. 2000. Study on convex-corner undercutting formed by masked-maskless etching in aqueous KOH. *J. Micromech. Microeng.* **10:** 309-313.

MARCHETTI, J., Y. He, O. THAN and S. AKKARAJU. 1998. Efficient process development for bulk silicon etching using cellular automata simulation techniques. Dalam *Symposium on Micromachining and Microfabrication, Micromachined Devices and Components,* hlmn. 86-92. Santa Clara, CA USA.

MERLOS, A., M. ACERO, M. BAO, J. BAUSSELS and J. ESTEVE. 1993. TMAH/IPA anisotropic etching characteristics. *Sensors and Actuators* A **37-38:** 737-43.

NOOR, M. M. 2004. Kajian punaran basah tidak isotropik secara eksperimen untuk fabrikasi membran silikon. Tesis Sarjana. Universiti Kebangsaan Malaysia, Bangi, Selangor.

PALIK, E. D., O. J. GLEMBOCKI, I. HEARD, P. S. BURNO and L. TENERZ. 1991. Etching roughness for (100) silicon surface in aqueous KOH. *Journal of Applied Physics* **70(6):** 3291-3300.

RUNYAN, W. R. 1965. *Silicon Semiconductor Technology*. New York: McGraw Hill.

SCHRODER, H., E. OBERMEIER and A. STECKENBORN. 1998. Effects of etching mask properties on the anisotrophy ration in anisotropic etching of {100} silicon on aqueous KOH. *J. Micromech. Microeng.* **8:** 99-103.

SEIDEL, H., L. CSEPREGI, H. HEUBERGER and H. BAUMGARTEL. 1990. Anisotropic etching of crystalline silicon in alkaline solutions I. *J. Electrochem. Soc.* **137:** 3612-26.

SHIKIDA, M., T. MASUDA, D. UCHIKAWA and K. SATO. 2001. Surface roughness of single-crystal silicon etched by TMAH solution. *Sensors and Actuators* A. **90:** 223-231.

SONPHAO, W. and S. CHAISIRIKUL. 2001. Silicon Anisotropic etching of TMAH solution. *ISIE 2001,* hlmn. 2049-2051, Pusan, Korea.

TABATA, O., R. ASAHI, K. FUNABASHI, K. SHIMAOKA and S. SUGIYA. 1992. Anisotropic etching of silicon in TMAH solutions. *Sensors and Actuators A* **34:** 51-57.

TELLIER, C. R. and S. S. DURAND. 1997. Micromachining of (hhl) silicon structures: experiments and 3D simulation of etched shapes. ***Sensors and Actuators*** A. **60:** 168-175.

ZAVRACKY, P. M. 1997. Comparative studies of TMAH and KOH for anisotropic etching of silicon. *Electrochem. Soc. Proc.* **97(5):** 102-117.

Pertanika J. Sci. & Technol. 14(1 & 2): 53 - 61 (2006)
ISSN: 0128-7680

The Concentration of Manganese, Copper, Zinc, Lead and Thorium in Sediments of Paka Estuary, Terengganu, Malaysia

Kamaruzzaman, B. Y., Willison, K. Y. S. & Ong, M. C.
Department of Marine Science,
Faculty of Science and Technology,
Kolej Universiti Sains & Teknologi Malaysia,
21030 Kuala Terengganu, Terengganu, Malaysia

Received: 30 July 2004

ABSTRAK

Sampel teras sepanjang 14 cm dari Sungai Paka telah diukur dengan peralatan ICP-MS bagi mendapatkan kepekatan Mn, Cu, Zn, Pb dan Th. Secara keseluruhannya, kepekatan semua logam didapati menurun mengikut kedalaman dan secara signifikannya mempunyai kepekatan yang tinggi di permukaan. Purata kepekatan Mn dan Cu adalah masing-masing 151.1 ± 59.1 mg/g berat kering dan 29.2 ± 6.9 mg/g berat kering, manakala Zn dan Pb mempunyai purata 72.5 ± 15.5 mg/g berat kering dan 54.9 ± 2.5 mg/g berat kering. Th pula didapati agak tidak sekata dan berada di antara 0.6 mg/g berat kering hingga 1.4 mg/g berat kering. Dalam kajian ini, hanya Mn dan Th mempunyai nilai faktor pengkayaan (EF) yang stabil dan ini boleh dianggap sebagai mempunyai sumber dominan secara semula jadi. Sebaliknya Cu, Zn dan Pb yang didapati mempunyai nilai EF yang lebih tinggi dan berkemungkinan mempunyai sedikit pengaruh kemasukan sumber-sumber antropogenik.

ABSTRACT

14 cm cores sediments from the Paka River were analyzed for Mn, Cu, Zn, Pb and Th using the inductively coupled plasma mass spectrometer (ICP-MS). Generally, the concentrations of all elements decreased with depth and have significantly higher concentration at the surface depth of the core. The concentration of Mn and Cu have average value of 151.1 ± 59.1 mg/g dry weights and 29.2 ± 6.9 mg/g dry weights, while Zn and Pb averaged at 72.5 ± 15.5 mg/g dry weights and 54.9 ± 2.5 mg/g dry weights, respectively. Th were slightly varied widely and ranged from 0.6 mg/g dry weights to 1.4 mg/g dry weights. In this study, only Mn and Th have enrichment factor (EF) values close to unity and may therefore be considered to be predominantly terrigenous in origin. On the contrary, the higher EF values found for Cu, Zn and Pb indicate that these metals might have some influenced from the anthropogenic input.

Keywords: Enrichment factor, heavy metals, ICP-MS, Paka River

INTRODUCTION

Estuarine areas where freshwater encounters seawater are characterized by a lateral variation in salinity, and can represent as a transfer box for the sediment between land and the open ocean (Meade 1972). They are very active areas

where a huge amount of organic matter and trace metals are introduced into the ocean system through river runoff, *in situ* primary production and anthropogenic impacts. Estuary appeared generally to be important sink for trace metal by the rivers of the world (Barry and Simon 1979). Heavy metal tend to be trapped in estuarine sediment are thus persist as a source of pollutants long after the cessation of discharges. The most comprehensive study was conducted by Davies *et al.* (1991) and reported the average concentration of heavy metal in sediment decreased in the order Zn > Pb > Cu > Cr > Ni > Cd between Newport Bridge and the river mouth. In estuarine systems, heavy metals in the water column have been observed to exhibit both conservative and non-conservative behavior along salinity gradients. In conservative systems, trace metals are simply diluted by increasing amounts of saltwater along the salinity gradient. In non-conservative systems, a host of different biogeochemical mechanisms have been shown to affect trace metal behavior in the water column. In non-conservative systems, surface complexation (and subsequent particle sedimentation) and desorption from particles can decrease the particulate fraction of metals along the salinity gradient (Flegal *et al.* 1991).

There are only limited information regarding to the geochemical profile of riverine system in Malaysia and only some initial research had been done by Kamaruzzaman *et al.* (2002) and Noor Azhar *et al.* (2003). In recent years, the study area especially for the first kilometer along the Paka River has been heavily impacted by discharges from municipal and industrial outflows. This was due to the rapid development of the area via expansion of the industrialization area as well as the increase in population. Steel and petro-chemicals are the main industry in this area and is the catalyst for other supportive industries to develop around the same area. The aim of this work was to study the geochemical behaviour of metals, their source and mode of incorporation in their sediments with regards to the sedimentological conditions of the area.

MATERIALS AND METHODS

Sampling Sites

The Paka River is located in the Dungun district, which situated near the Paka town, southern of Kuala Terengganu, the capital state of Terengganu (*Fig. 1*). The study area lies in the wet tropics where high rainfall is recorded in the monsoon season with a high rainfall were recorded in the month of November and January. The length of Paka River is approximately 87 km long and with total catchment area of approximately 830 km^2. It extends and enlarges westerly from the mouth before turning south, bordering the smaller Kertih River catchments on the east (*Fig. 1*). The inland and mountainous regions of the catchments are mainly covered with natural tropical rain forest. The vegetation of both coastal breaches appear to be a mixture of grass and low scrub-land truncated in a north-south direction by long and narrow swamps which provide drainage to the revised beaches.

Analytical Method for Metals

In this study a 14 cm sediment core was collected by using the D-section corer in the Paka estuary (*Fig. 1*). The core was cut into segments of approximately 5 cm interval, labeled and stored until analysis in the laboratory. The sediment samples were digested according to the published methods by several researchers (Noriki *et al.* 1980; Sen Gupta and Bertrand 1995; Kamaruzzaman 1999) with some modifications. An inductively-coupled plasma mass spectrometer (ICP-MS) was used for the quick and precise determinations of Mn, Cu, Zn, Pb and Th in the digested marine sediment. Briefly, the digestion method involved the heating of 50 mg of a < 63 μm size sample in a sealed teflon vessel with mixed concentrated acids of HF, HNO_3 and HCl in the ratio of 2.5 : 3.5 : 3.5. The teflon vessels were kept at 150 ^{0}C for 3 – 5 hours. After cooling, a mixed solution of boric acid and EDTA was added, and the vessel was again heated at 150 ^{0}C for at least 5 hours. After cooling to room temperature, the content of the vessel was thoroughly transferred into a 10 ml polypropylene test tube and was diluted to 10 ml with deionized water. A clear solution with no residue should be obtained at this stage. The precision assessed by replicate analyses was within 3%. The accuracy was also examined by analyzing, in duplicate a Canadian Certified Reference Materials Project standard (DL-1a) and the results coincided with the certified values within a difference of ± 3%.

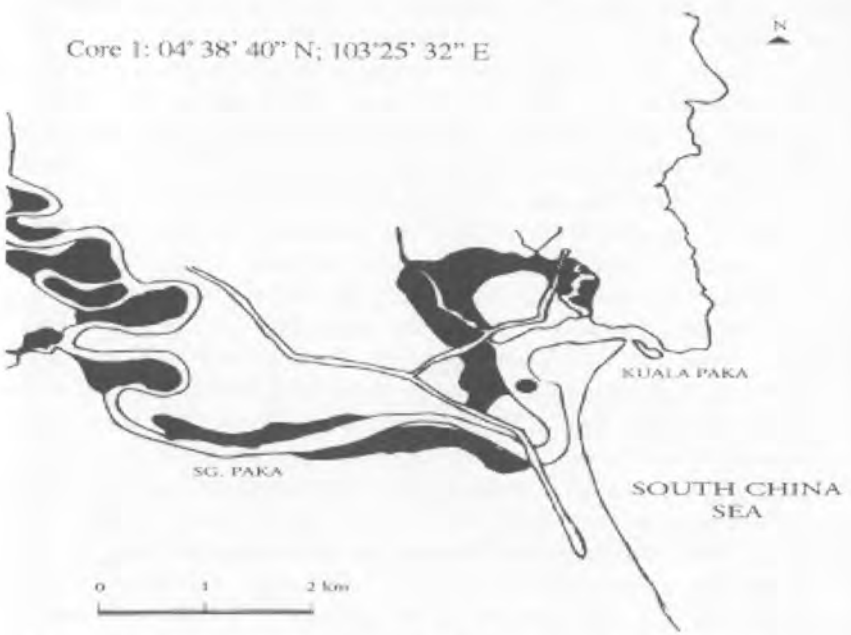

Fig. 1: Location of the core (•) study area in the Paka Estuary, Terengganu, Malaysia

RESULTS AND DISCUSSION

Depth profiles of Mn, Cu, Zn, Pb and Th are given shown in *Fig. 2*. Generally, the concentrations of heavy metal recorded in this study were generally below the levels of most polluted estuaries, even though some high content of metals were discovered at several depths. Although no specific trend was identified, the concentrations of metals were relatively lower in the surface depth compared to the deeper depth. Since the study areas is located in an enclosed estuary with less industrial activities, the input of some high concentration of metals might have come from town residential areas, city sewage effluents and the fisheries activities. In this study, Mn ranged from 110 mg/g dry weights to 280 mg/g dry weights and averaged at 210 mg/g dry weights. The average Mn concentration was much lower than values of the global average shales (Martin and Meyback 1979), but is greater compared to the Mn content in Johor Straits (Khalik *et al.* 1997). The existence of the subsurface maxima of Mn are caused by the migration of Mn^{2+} with interstitial water and subsequent precipitation as a kind of carbonate on the surface of volcanic pumice (Tsunogai *et al.* 1979). A subsurface maximum in the Mn content within the enriched layer has also been observed in continental shelf sediments (Hartman *et al.* 1979) and is common in pelagic sediments (Wangersky 1962). The depth profile of Zn was generally contants ranging from 50 mg/g dry weights to 100 mg/g dry weights. Their average concentrations are about the values of the global average shales (Martin and Meyback 1979). Most of the Zn found in the sediments is of natural origin which was probably derived from the weathering of ultramafic rocks. However, some higher concentrations at certain depth were assumed as a contribution of anthropogenic activities that especially near the vicinity of the fishing port and the shipyard. The painting activities of the fishing boat and the use of anti-rust paint in the fishing industry may effects the concentration levels of Zn in the sediments. Depth profiles of Cu show more or less the same pattern as Zn, ranging from 15 mg/g dry weights to 50 mg/g dry weights. In general, their concentration showing an increase trend with depth. The enhanced Cu concentrations found in the surface sediment reflected the increase of concentration in the exchangeable fraction (Johanna 2002). However, some relative low concentration of metals at the deeper depth might be due to the lack of supply of rich material and the presence of a high load of organic material, derived from planktonic species in the study areas.

Meanwhile for Pb, their concentration ranged from 50.6 mg/g dry weights to 60.6 mg/g dry weights and averaged at 54.4 mg/g dry weights. The average Pb concentration was about the values of the global average shales (Martin and Meyback 1979). Pb was generally constant with depth but showed enrichment in the top few centimeters of the core. Although anthropogenic inputs are supposed to be the major source for the increased Pb concentrations found in the study area, an increase due to diagenetic changes cannot be excluded, being a common phenomenon in the sediments. Furthermore, Pb is mostly supplied to the open marine environment by atmospheric inputs, and was used as an excellent tracer to study historical pollution records. Finally, the depth

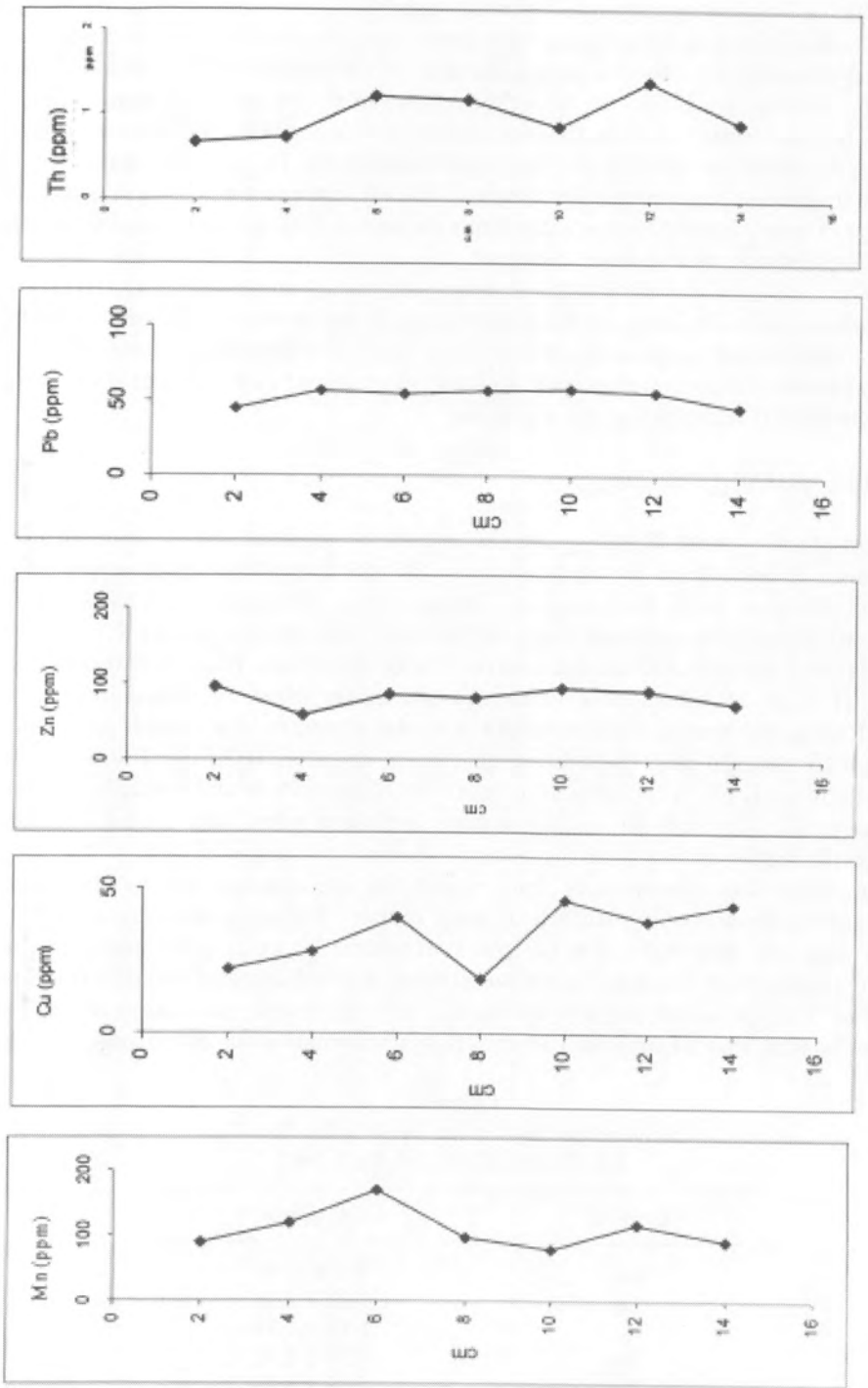

Fig. 2: Vertical profiles of the concentration of Mn, Zn, Pb and Th against depth

profile of Th were varied with highest concentration was observed at the depth of 12 cm (1.4 mg/g dry weights) and lowest was found at the surface depth (0.6 mg/g dry weights). In rivers, distribution or the inputs of Th is unstable and were much influenced by the water movement of fluvial and tidal, water velocity and the monsoon seasons that occurred in the study areas. According to Kamaruzzaman *et al.* (2001), the high content of Th probably cause from erosion process from monazite mineral. Mostly, the content of Th is constants where it was produced constantly from its parent ^{234}U solubility and disperses homogeneously in the water column.

For a better estimation of anthropogenic input, an enrichment factor was calculated for each metal by dividing its ratio to the normalizing element by the same ratio found in the chosen baseline. Table 1 shows the calculated EFs of the analysed elements with respect to those determined in the crustal abundance (Taylor 1964), employing the equation:

$$EF = (E/Al)_{sed}/(E/Al)_{crust},$$

where $(E/Al)_{sed}$ and $(E/Al)_{crust}$ are the relative concentrations of the respective element E and Al in the sediment and in the crustal material, respectively (Molinari *et al.* 1993; Kremling and Strue 1993). An enrichment factor close to 1 would indicate a crustal origin, while those with factors greater than 10 are considered to have non-crustal sources. It is clear from Table 1 that only Mn and Th have EF values close to unity and may therefore be considered to be predominantly terrigenous in origin. On the contrary, the higher EF values found for Cu, Zn and Pb indicate that these metals can be considered to be predominantly anthropogenic in origin. In other study near Chukai-Kemaman estuary, Cu, Zn and Pb in the surface sediment were also found to have relatively higher values near the estuary (Kamaruzzaman *et al.* 2002). In these areas, enormous amounts of finer sediments are transported by the river, increasing the adsorbing surface of trace metals. Kamaruzzaman *et al.* (2002) also reported that there is a positive correlation between grain size and the concentrations of Cu, Zn and Pb, suggesting the influence of the fine fraction in their incorporation into the sediments. The fairly well correlation of Cu, Zn and Pb, with that of organic carbon (Kamaruzzaman *et al.* 2004) suggests the

TABLE 1
Calculated average values of EF"s for Mn, Cu, Zn, Pb and Th in the study area

Element	EF values
Mn	0.5 ± 0.24
Cu	1.21 ± 2.50
Zn	1.72 ± 1.74
Pb	3.27 ± 4.94
Th	0.18 ± 0.08

association of these metals with organic material. The accumulation of organic material in the area not only providing the adsorbing surfaces but in addition, the reducing environment formed prevents their possible remobilization.

ACKNOWLEDGEMENTS

This research was conducted with joint funding from the Malaysia Ministry of Science and Technology under the Intensified Research for Priority Areas (IRPA) project number 55007. The authors wish to express their gratitude to Oceanography Laboratory teams for their invaluable assistance and hospitality throughout the sampling period.

REFERENCES

BARRY, T. H. and H. R. SIMON. 1979. Trace metal speciation in the freshwater and estuarine region of the Yarra River, Victoria. Water Studies Centre, Caulfield Institute of Technology, Caulfield East, Australia.

DAVIES, C. A. L., K. TOMLINSON and T. STEPHENSON. 1991. Heavy metal in River Tee Estuary sediments. *Environmental Technology* **12**: 961-972.

FLEGAL, A. R., G. J. SMITH, S. SANUDOWITHELNY and L. C. D. ANDERSON. 1991. Dissoved trace element cycles in the San Francisco Bay Estuary. *Mar. Chem.* **36**: 329 – 363.

HARTMAN, M., P. J. MULLER, E. SUESS and C. H. VAN DER WEIJDEN. 1979. Chemistry of late quarternary sediments and their interstial waters from the NW African continental margin. *Meteor* **24**: 1–67.

JOHANNA, A. S. 2002. Final Year report, Bachelor Science (Marine Science), Faculty of Applied Science and Technology, Universiti Putra Malaysia Terengganu. 71p.

KAMARUZZAMAN, B. Y. 1999. Geochemistry or the marine sediments. Its paleoceanographic significance. Ph.D Thesis. Submitted to Hokkaido University. 143p.

KAMARUZZAMAN, B. Y., T. JAMIL and S. HASRIZAL. 2004. Organic carbon in sediments and particulate organic carbon in water of the Chukai-Kemaman Estuarine System. *Journal of BioScience* **15(1)** (In Press).

KAMARUZZAMAN, B. Y., M. L. HUSAIN, N. A. M. SHAZILI, I. SULONG and K. A. RASHID. 2002. Study on the distribution of some heavy metals and pollution status of a tropical microtidal river: The Chukai-Kemaman River, Terengganu, Malaysia. *Dimensions of Pollution* **1**: 115–130.

KAMARUZZAMAN, B. Y., Y. ROSNAN, H. MOHD LOKMAN, N. A. M. SHAZILI and A. NOR ANTONINA. 2002. Physico-chemical characteristics and dissolved trace metals in the Chukai River Estuary, Terengganu, Malaysia. *Chemical Research Communication* **25**: 41 – 51.

KAMARUZZAMAN, B. Y., H. SUHAIMI, E.K. TEH, H.F. LEONG, K.H. SOON and K. Y. CHONG. 2001. The determination of ^{230}Th in the sediments: Sedimentation in the mangrove Forests of Pulau Sekeping, Kemaman, Terengganu. *Journal of Ultra Scientist of Physical Sciences* **13(2)**: 239–245.

KHALIK, H. W., A. ZAHARUDIN, A. M. S. NOOR, Y. ROSNAN and R. CARPENTER. 1997. Geochemistry of sediment in Johor Strait between Malaysia and Singapore. *Continental Shelf Research* **17(10):** 1207-1228.

KREMLING, K. and P. STREU. 1993. Saharan dust influence trace element fluxes in deep North Atlantic subtropical waters. *Deep Sea Research* **40**: 1155 – 1168.

MARTIN, J. M. and M. MEYBACK. 1979. Elemental mass balance of material carried by major world rivers. *Marine Chemistry* **7**: 173 – 206.

MEADE, R. H. 1972. Transport and deposition of sediments in estuaries. *The Geological Society of American Members* **133:** 91-117.

MOLINARI, E., S. GUERZONI and G. RAMPAZZO. 1993. Contribution of Saharan dust to the central Mediterranean Basin. *Geological Society of America* Special Paper **284**: 303 – 312.

NOOR AZHAR, M. S., B. Y. KAMARUZZAMAN, Y. ROSNAN and A. NOR ANTONINA. 2003. Speciation of Cu, Pb and Zn in sediments of Ibai Estuary, Kuala Terengganu, Malaysia. *Dimensions of Pollution* **2**: 43-52.

NORIKI, S. K., NAKANISHI, T. FUKAWA, M. UEMATSU, T. UCHIDA and S. TSUNOGAI. 1980: Use of a teflon vessel for the decomposition followed by the determination of chemical contituents of various marine samples. *Bull. Fac. Fish,* Hokkaido Univ. **31**: 354 - 465.

SEN GUPTA, J. G. and N. B. BERTRAND. 1995. Direct ICP-MS determination of trace and ultratrace elements in geological materials after decomposition in a microwave oven, quantitation of Y, Th, U and lanthanides. *Talanta* **42**: 1595-1607.

TAYLOR, S. R. 1964. Abundance of chemical elements in the continental crust: a new table. *Geochimica et Cosmochimica Acta* **28**: 1273 – 1285.

TSUNOGAI, S., I. YONEMARU and M. KUSAKABE. 1979: Post depositional migration of Cu, Zn, Ni, Co, Pb and Ba in deep sea sediments. *Geochem. J.* **13**: 239 - 252.

WANGERSKY, P. J. 1962. Sedimentation in three carbonate cores. *J. Geol.* **70**: 364 – 375.

Pertanika J. Sci. & Technol. 14(1 & 2): 61 - 74 (2006)
ISSN: 0128-7680

Deformation and Shear Strength Characteristics of Some Tropical Peat and Organic Soils

Bujang B. K. Huat
Department of Civil Engineering
Faculty of Engineering, Universiti Putra Malaysia
43400 Serdang, Selangor, Malaysia
E-mail:bujang@eng.upm.edu.my

Received: 26 March 2004

ABSTRAK

Tanah-tanah gambut dan organik lazimnya terdapat sebagai endapan yang tersangat lembut, yang merupakan sebahagian daripada sistem tanah berair. Tanah-tanah ini boleh juga terdapat sebagai stratum di bawah endapan tanah yang lain. Tanah-tanah ini lazimnya dikategorikan sebagai tanah bermasalah oleh kerana ia tersangat boleh mampat serta mempunyai kekuatan ricih yang sangat rendah. Di beberapa negara seperti Malaysia, tanah sebegini terdapat dengan banyaknya. Oleh yang demikian penggunaan kawasan-kawasan sebegini semakin diperlukan dengan berkurangnya kawasan-kawasan lain yang lebih sesuai. Dengan itu parameter kejuruteraan serta kaedah pembinaan yang bersesuaian perlu dicari. Kita perlu mengembangkan pengatahuan kita mengenai tanah-tanah sebegini, khususnya dari aspek kejuruteraan seperti kebolehmampatan dan kekuatan ricih tanah. Kertas kerja ini memerihalkan kajian yang telah dijalankan di makmal dan juga di lapangan mengenai ubah bentuk dan kekuatan ricih tanah organik dan gambut tropika. Sampel-sampel tanah diambil di beberapa lokasi di Malaysia, Johor, Perak, Sarawak dan Selangor. Tanah-tanah ini mempunyai kandungan organik yang berjulat di antara 50% hingga 95%. Indeks mampatan tanah didapati bertambah dengan bertambahnya kandungan organik dan air tanah. Manakala kekuatan ricih tanah berkurangan dengan bertambahnya kandungan organik dan air tanah. Kekuatan ricih tanah turut didapati dipengaruhi oleh darjah pereputan tanah. Tanah dengan serat yang tinggi mempunyai kekuatan ricih yang tinggi.

ABSTRACT

Peat and organic soils commonly occur as extremely soft, unconsolidated surficial deposits that are an integral part of the wetland systems. They may also occur as strata beneath other surficial deposits. These soils are problematic as they are very highly compressible and are of very low shear strength. In countries like Malaysia, peat and organic soils are found in abundance. Utilization of this marginal ground is required in increasing number of instances in the recent years. Hence suitable geotechnical design parameters and construction techniques needed to be found for this type of ground condition. This paper presents results of laboratory and field tests on the deformation and shear strength characteristics of tropical organic and peat soil. The soil samples were collected from several locations in Malaysia, namely from the states of Johore, Perak, Sarawak and Selangor. These soils represented tropical peat and organic soils with organic content ranging from 50% to 95%.

The soil compression index is found to increase with increase in the organic content and natural moisture content. While for case of undrained strength, the shear strength of tropical peat and organic soil is found to decrease with increase in the organic content and natural moisture content. The shear strength of the soil is also dependent on the degree of humification of the soil, with more fibrous soils having higher undrained strength.

Keywords: Deformation, index properties, organic soil, peat, shear strength

INTRODUCTION

Peat and organic soils commonly occur as extremely soft, wet, unconsolidated surficial deposits that are integral parts of the wetland systems. They may also occur as strata beneath other surficial deposits (Jarrett 1995). These soils are found in many countries throughout the world. In the US peat is found in 42 states with a total acreage of 30 million hectares. Canada and Russia are the two countries with a large area of peat, 170 and 150 million hectares respectively (Hartlen and Wolski 1996). For the case of tropical peat, or tropical peat lands, the total world coverage is about 30 million hectares, two thirds of which are in Southeast Asia. Malaysia has some 3 million hectares - about 8% of the land area is covered with tropical peat. While in Indonesia peat covers about 26 million hectare of the country land area, with almost half of the peat land total is found in Indonesia's Kalimantan.

Peat actually represents an accumulation of disintegrated plant remains, which have been preserved under condition of incomplete aeration and high water content. It accumulates wherever the conditions are suitable, that is, in areas with excess rainfall and the ground is poorly drained, irrespective of latitude or altitude. Nonetheless, peat deposits tend to be most common in those regions with comparatively cool wet climate. Physico-chemical and biochemical process cause this organic material to remain in a state of preservation over a long period of time. In other words, waterlogged poorly drained condition, not only favor the growth of particular type of vegetation but also help preserve the plant remains.

These soils are generally referred to as problematic soils due to their high compressibility and low shear strength. Access to these superficial deposits are usually very difficult as the water table will be at, near or above the ground surface. Undoubtedly, these are the consequences of the tendency to either avoid construction and buildings on these soils, or when this is not possible, to simply remove, replace or displace them, that in some instances may lead to possibly uneconomical design and construction alternative. However in many countries including Malaysia, substantial areas are covered by this material. The thickness of this deposit varies from just about 1 m to more than 20 m thick. Pressures on the land use by industry, housing and infrastructure are leading to more frequent utilization of such marginal grounds. It is therefore necessary to expand the knowledge of their geotechnical properties and mechanical behavior, in particular those in relation to their deformation and shear strength

characteristics, and subsequently devises suitable design parameters and construction techniques on these materials.

Review of literature indicates that peat and organic soils are very variable in their properties, both from one deposit to another and from point to point in the same deposit. Such variations are associated with the origin of these soils, the type of plant from which they are derived, the mineral content of the deposit and the amount of decay or humification that had occurred. All these features are reflected in the mechanical behavior (compressibility and shear strength) with which the geotechnical engineer is concerned (Tresidder 1966). When a soil is subjected to an increase in compressive stress due to foundation load, the resulting soil compression (generally called settlement) generally consists of elastic compression (immediate settlement), primary compression (consolidation settlement) and secondary compression. Compared with mineral soils, peat soils are highly organic and highly compressible. Its compression or settlement process may take a considerably longer amount of time. Peat generally posses low undrained strength and high compressibility. Buildings on peat are usually suspended on piles, but the ground around it may still settle, creating a scenario as depicted in *Fig.1* below.

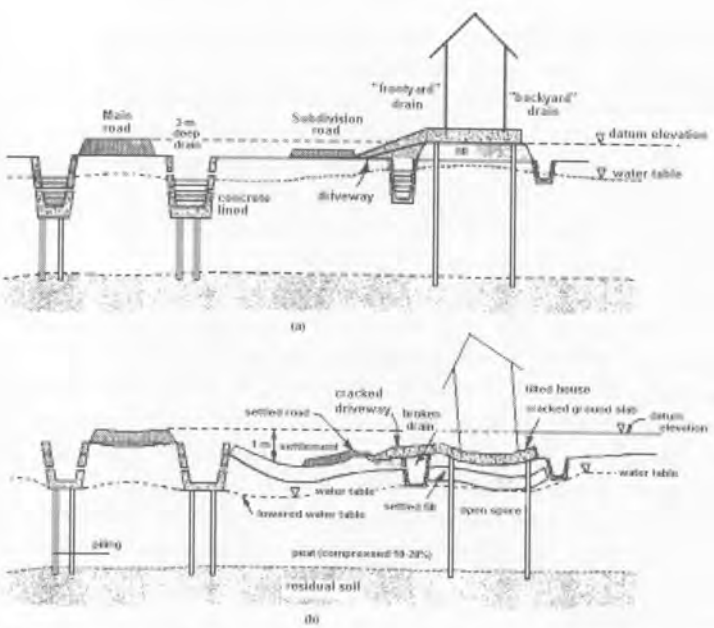

Fig. 1: (a) Typical section of a housing estate on peat (immediately after completion of construction) (b) Several years after completion of construction (scale exaggerated)

The calculation of the settlement requires evaluation of soil parameters from the compression curves which are usually obtained from laboratory oedometer tests. The results of incremental loading oedometer tests are usually

presented as the relationship between void ratio, e, and effective vertical stress, σ_v. The vertical effective stress may be plotted on a linear scale to determine the coefficient of volume change, m_v, and oedometer modulus, M, or on logarithmic scale to determine the compression index, c_c.

As with mineral soils (silt and clay), the settlement parameters of peat (i.e. consolidation settlement) may also be determined from standard incremental oedometer (one dimensional compression) tests (Edil 1997). The parameters are interpreted from traditional e - log σ_v plots. There may be differences in the magnitudes of various quantities measured but the general shape of the consolidation curves appear reasonably similar and the formulation developed for clay compression can be used to predict the magnitude and rate of settlement (Edil 1997).

There are however a certain class of peat, typically peat with high organic and fibre content with low degree of humification, that do not conform to the concept of conventional clay compression because of their different solid phase properties and microstructures. The analysis of compression of such materials present certain difficulties when conventional methods are applied because the curves obtained from the conventional oedometer tests and behaviour exhibited by them may show little similarity to the clay behaviour (Edil 1997; Den Haan 1997).

When conducting laboratory test, great care should be taken in determining the deformation parameters of these soils for the settlement calculations. Usually the laboratory consolidation tests are time consuming, rather expensive and require great care in handling and interpreting the results. Considering the above-mentioned factors, an effort has been made to correlate the compression index of these soils to some other easily determined soil index properties. There are a number of correlations for clays, but very few for organic soils. This is the focus of this paper.

Shear strength is another important parameter in soil mechanics. Shear strength always play a vital role when engineering decision comes across with any soils including peat. Shear strength is a concern both during construction for supporting construction equipment as well as at the end of construction in supporting the structure. Low shear strength and high compressibility of the peat soils however confined them in the problematic category. Accuracy in determining the shear strength of these soils is associated with several variables namely; origin of soil, water content, organic content and degree of humification. For the case of peat, the presence of fibers modifies our concepts of strength behavior in several ways. It can provide effective stress where there is none and it induces anisotropy.

Early research on peat strength indicates some confusion as to whether peat should be treated as a frictional material like sand or cohesive like clay. Commonly, surficial peats are encountered as submerged surficial deposits. Because of their low unit weight and submergence, such deposits develop very low vertical effective stresses for consolidation and the associated peat exhibit high porosities and hydraulic conductivities comparable to those of fine sand

or silty sand (Dhowian and Edil 1980). Such a material can be expected to behave "drained" like sand when subjected to shear loading. However, with consolidation, porosity decreases rapidly and hydraulic conductivity becomes comparable to that of clay. There is a rapid transition immediately from a well-drained material to an undrained material (Edil *et al.* 1994).

Determination of shear strength parameters for organic soils, as with other soils, is important and somehow a difficult job in geotechnical engineering. For organic soils, several methods have been used to determine the undrained shear strength in the laboratory namely Swedish fall-cone test, triaxial test, shear box test and vane shear test. For the case of field tests, field vane and Dutch Cone Penetration tests are often used.

TEST PROGRAMS

A series of laboratory and field test have been carried out to study the deformation and shear strength characteristics of tropical peat and organic soils.

For the study on deformation, samples were collected from nine different locations in the state of Johore, Perak, Sarawak and Selangor, generally at depth between 0.5 m – 1.0 m below the ground surface. The organic content of the samples range from 50 % to 95 %, with natural water content in the range of 200 % – 800 %, and liquid limit of 150 % to 400%. In terms of Van Post scale (Landva and Pheeney 1980), the samples were *H5* to *H9*, that is hemic to sapric peat. The consolidation characteristics of the samples were determined from standard incremental oedometer tests, with sample size of 75 mm diameter and 20 mm high, and applied normal stress of 5 kPa to 160 kPa. The consolidation parameters were interpreted from the traditional e- log σ_v plots.

For the study on shear strength, both laboratory and field tests were carried out. Several peat and organic soil samples were collected and tested for their undrained shear strength using laboratory shear box test with sample size of 60 mm x 60 mm by 25mm thick. The samples are generally obtained at depth of 0.5m below the ground level. In situ tests were also performed on the same site using a small (50 mm diameter) field vane shear at depth of about 0.5 m below ground surface. The samples were collected from five different locations in Selangor and Negeri Sembilan. The organic content of the sample range from 79 % – 98 %, with liquid limit of 160 % – 377 %, and water content of 200 % - 800 %. In order to examine the effect of degree of humification on the soil shear strength, tests were done on samples with Van Post scale (Landva and Pheeney 1980) ranging from *H1* to *H10*, that is from fibric to hemic to sapric peat.

TEST RESULTS AND DISCUSSION

Deformation Characteristics

(i) Compression Index, c_c and Liquid Limit, w_l

An effort is made to correlate compression index, c_c, with liquid limit, w_l, void ratio, e_o, and ratio of c_c / $(1+e_o)$.

The plot of compression index, c_c, versus the liquid limit of the soil shows that c_c increases with the liquid limit (w_L) of the soil as shown in *Fig. 2*. Farrell *et al.* (1994) considered the empirical relationship between the compression index and the liquid limit suggested by Skempton and Petley (1970) for organic soils (equation 1) as to give a reasonable approximation of this parameter. Hobbs (1986) estimated the compression index for fen peat using equation 2, which gave a slightly lower value of c_c. Values of c_c of tropical peat samples tested however were apparently a little higher than the above two relationships (*Fig. 2*).

$$c_c = 0.009(w_L - 10) \tag{1}$$

$$c_c = 0.007(w_L - 10) \tag{2}$$

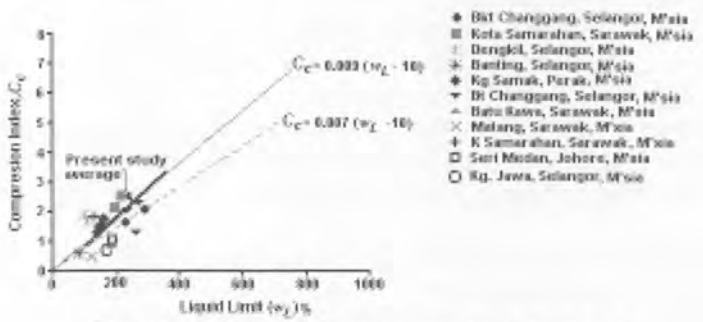

Fig. 2: Compression index (c_c) versus liquid limit (w_L)

The c_c values of the tropical peat studied range from 1 to 3, much higher than sedimentary soil such as clay whose c_c is only 0.2 – 0.8. It is of interest to note that the c_c of the Irish peat range from 1 – 4, as shown in *Fig. 3*, which is quite close to the tropical peat.

Azzouz *et al.* (1976) reported the following relationship for organic soil and peat,

$$c_c = 0.0115\ w \tag{3}$$

Where w is soil natural water content in percent. Note that the natural water content of the peat studied range from 200 % – 800 %. Using the above equation, this would give c_c of 2 – 9, which is higher than the measured values.

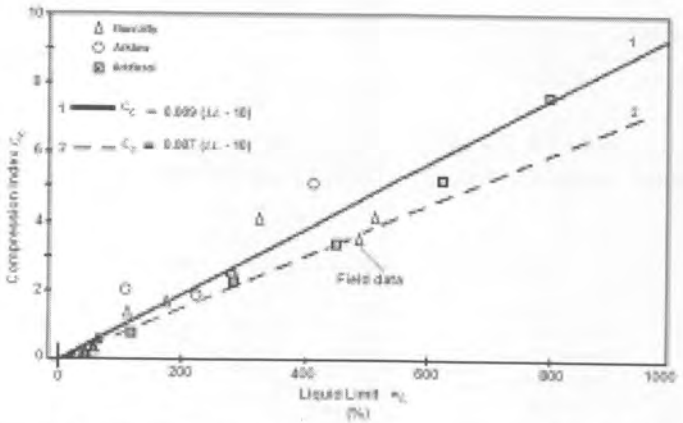

Fig. 3: Compression index (c_c) - liquid limit (w_l) (Farrel et al. 1994)

(ii) Void Ratio with Liquid Limit and Natural Water Content

Fig. 4 shows a plot of the initial void ratios versus liquid limits of the peat and organic soils from several sites in Malaysia together with the normally consolidated peat found by Miyakawa (1960), and Skempton and Petley (1970). The figure shows an increasing trend in void ratio with the increase of the soil liquid limits. Void ratio of the tropical peat studied is found to range from 1.5 – 6, that is

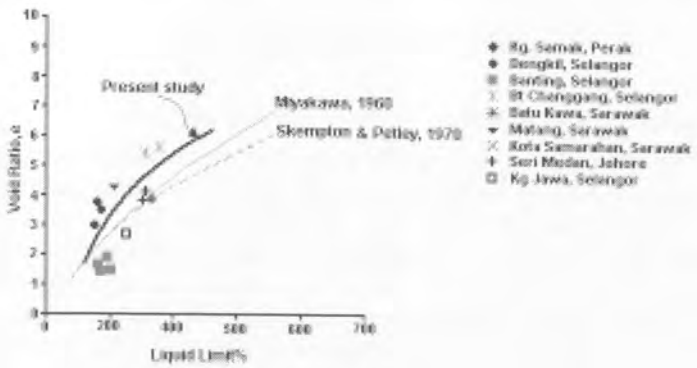

Fig. 4: Relationship between the void ratio and liquid limit

for the case of amorphous peat. For the case of fibrous peat it can be as high as 25. Such high void ratios gives rise to phenomenally high water contents. For comparison, Malaysian marine clay for instance, has an initial void ratio in the range of 1.5 to 2.5. The natural void ratios of the peat indicate their higher compressibility.

Fig. 5 shows the graph of void ratio (e_o) and natural water content (w_o). The best-fit line in the above figure is expressed by:

$$e_o = \frac{30.65(w_o + 0.88)^{0.116} - 30}{1.12} \tag{4}$$

As for the case with liquid limit, void ratio increases with increase in natural water content. A similar trend of behavior is observed by Den Haan (1997).

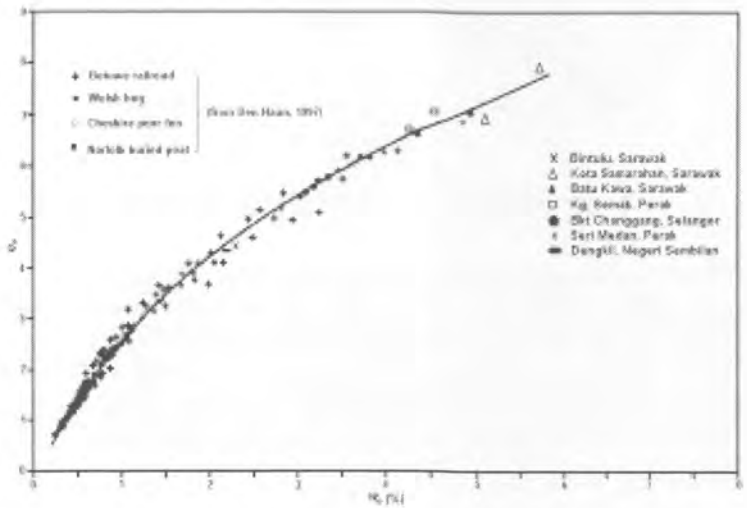

Fig. 5: Initial water content-void ratio

(iii) Compression Index Ratio, $c_c/(1+e_o)$, and Liquid Limit

Hobbs (1986) found that despite the large variations, which occur within peat and organic soils, the variation in the ratio of $c_c/(1+e_o)$ is relatively small. The values of this ratio determined from the laboratory test on tropical peat soil samples are plotted in *Fig. 6.* In agreement with Hobbs observation, the trend obtained is similar to the other researches. However the compression index ratios, $c_c/(1+e_o)$, of the tropical peat are generally slightly higher than the others. This is likely due to their higher in situ void ratio (e_o). The value of e_o depends on the in situ vertical stress; hence e_o must be that appropriate to the very low effective stress conditions.

Shear Strengths of Tropical Peat and Organic Peat Soil

(i) Shear Box Test

The results obtained from the shear box tests are shown in Table 1. The results show that the shear strengths of the peat and organic soils are very low. From the shear box test, it was found that the soils have low cohesion, (c_u), with values in the range of 6 to 17 kPa. The angle of internal friction, (ϕ_u), ranges from 3° to 20°. The ϕ_u values are generally lower with increasing degree of humification.

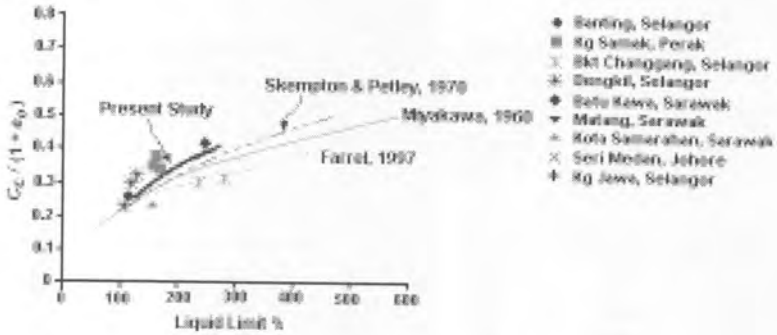

Fig. 6: Relationship between $c_f/(1+e_o)$ and the liquid limit

Similar trend is also observed for cohesion. A typical normal and shear stresses plot of the shear box test is shown in *Fig. 7.*

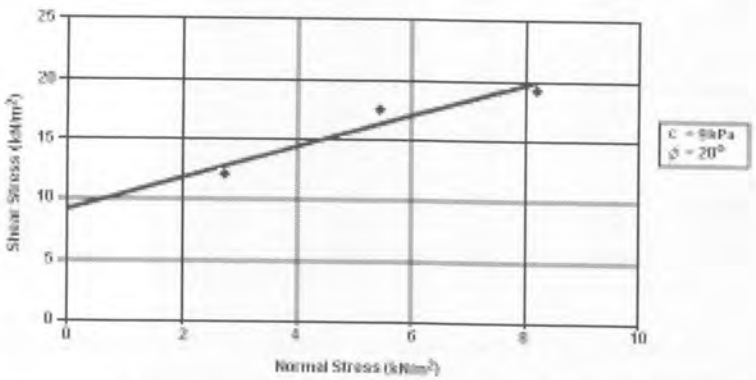

Fig. 7: Typical relationship between shear stress and normal stress for sample with high fibrous content (H1) (sample location: Banting, Selangor, Malaysia)

(ii) Field Vane Test

From the vane shear test, the undrained strength of the soils were found to range from 3 kPa -15 kPa (Table 2).

The plot of moisture content against vane shear strength portrays a decreasing behaviour of shear strength with increasing moisture content, as shown in *Fig. 8.* At the same moisture content, the high fibrous (*H1-H3*) peat gives higher strength compared with the medium and low fibrous (*H4-H10*) peat. In general, the high fibrous or fibric (*H1 - H3*) peat has higher shear strength than the medium fibrous or hemic (*H4 – H6*) peat and the low fibrous or sapric (*H7 – H10*) peat. The behaviour is more or less the same when vane shear strength is plotted against organic content, *Fig. 9.* According to Mitchell (1993), the effect of organic matter and stiffness of soils depends largely on whether

TABLE 1
Basic soil properties and laboratory shear box test results of some tropical peat and organic soils

Location	Moisture content	Organic content	Liquid limit	Van Post scale	Cohesion (kPa)	Angle of internal friction (deg)
Banting, Selangor	211	85	294	H1	9-11	9-20
	219	94	316	H6	11-12	9-12
	802	83	362	H10	6-10	12-20
Banting, Selangor	195	79	219	H2	6-11	9-16
	832	84	361	H5	8-10	7-10
	225	85	166	H8	8-12	6-11
Kg. Jawa, Klang	215	78	180	H3	10-12	6-14
	209	89	325	H6	12-14	7-25
	786	85	368	H8	7-11	8-13
Kg. Jawa, Klang	680	85	298	H3	11-12	10-15
	747	93	352	H5	10-12	5-10
	720	83	282	H7	7-9	9-12
Dengkil, N. Sembilan	246	98	305	H2	13-17	3-12
	301	98	335	H5	11	13-15
	786	83	377	H8	8-9	12-20

the organic matter is decomposed or consist of fibres which can act as reinforcement.

According to Van Post scale (Landva and Pheeney 1980), the degree of humification is graded on scale from 1 to 10 and designated from *H1* to *H10*. *Fig. 10* shows the decreasing trend between the degree of humification and the vane shear strength. The shear strength obtained from vane shear strength test decreases gradually with high degree of the humifications.

Fig. 11 shows the field vane shear data, measured with the larger (100 mm diameter) vane, from a new mosque project site at Putrajaya, Malaysia. There is only a slight tendency for an increase in strength with depth. The low bulk density of peat together with high water table implies low effective stresses with depth. Because of this there may not be a discernible increase of strength with depth within the peat layer (0.5 m – 4.0 m).

The field vane shear strength seems to relate well with results obtained using the small vane shear, for soil with a similar degree of humification as shown in *Fig. 10* above.

Yogeswaran (1995) reported the average field vane shear strength for tropical peat found in Sarawak to be only 10 kPa while the sensitivity ranges

TABLE 2
Basic properties and vane shear strength parameters of some tropical peat and organic soils

Location	Moisture content	Organic content	Liquid limit	Van Post scale	Field vane shear strength (kPa)
Banting, Selangor	211%	85%	294%	H1	10 – 12
	219%	94%	316%	H6	7 – 9
	802%	83%	362%	H10	4 – 6
Banting, Selangor	195%	79%	219%	H2	11
	832%	84%	361%	H5	10
	225%	85%	166%	H8	4
Kg. Jawa, Klang	214%	79%	180%	H3	11
	225%	84%	325%	H6	8
	618%	88%	368%	H8	5
Kg. Jawa, Klang	680%	85%	298%	H3	10 – 15
	747%	93%	352%	H5	5 – 10
	720%	83%	282%	H7	9 – 12
Dengkil, N. Sembilan	246%	98%	305%	H2	9 - 13
	301%	98%	335%	H5	6 - 10
	786%	83%	377%	H8	3 - 6

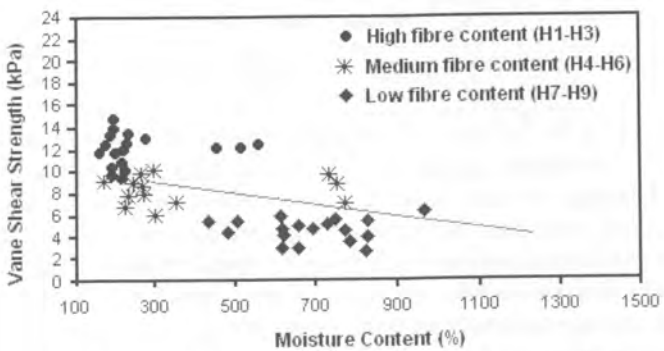

Fig. 8: Plot of vane shear strength versus moisture content

the degree of humification of the soils, with more fibrous soils having higher undrained strength.

REFERENCES

AZZOUZ, A.S., KRIZEK, R.J. and R.B. COROTIS. 1976. Regression analysis of soil compressibility. *Soils and Foundation* **16(2):** 19-29.

DEN HAAN, E. J. 1997. An overview of the mechanical behaviour of peats and organic soils and some appropriate construction techniques. In *Proceedings of Conference on Recent Advances in Soft Soil Engineering*, ed. Huat and Bahia, p. 17-45. Kuching, Sarawak, Malaysia.

DHOWIAN, A.W. and T.B. EDIL. 1980. Consolidation behavior of peats. *ASTM Geotechnical Testing Journal* **3(3):** 105-114.

EDIL, T.B, P.J. FOX and L.T. LAN. 1991. End-of-primary consolidation of peat. *Tenth ECSMFE*, Florence **1:** 65-68.

EDIL, T.B. and X. WANG. 2000. Shear strength and K_o of peats and organic soils. In *Geotechnics of High Water Content Materials*, ed. Edil and Fox, p. 209-225. ASTM STP 1374 American Society for Testing and Materials.

FARRELL, E.R. 1997. Some experience in the design and performances of roads and road embankment on organic soils and peats. In *Proceedings of Conference on Recent Advances in Soft Soil Engineering*, ed. Huat and Bahia, p. 66 – 84. Kuching, Sarawak, Malaysia.

FARRELL, E.R., C. O'NEILL and A. MORRIS. 1994. Changes in the mechanical properties of soils with variation in organic content. In *Advances in Understanding and Modeling the Mechanical Behaviour of Peat*, p. 19-25. Balkema Rotterdam.

HARTLEN, J. and J. WOLSKI. 1996. *Embankments on Organic Soils.* Elsevier.

HOBBS, N. B. 1986. Morphology and the properties and behaviour of some British and foreign peats. *Quaterly Journal of Engineering Geology* **19:** 7–80.

JARRETT, E.P.M. 1995. Geoguide 6. Site investigation for organic soils and peats. Jabatan Kerja Raya (PWD), Malaysia.

LANDVA, O.A. and P.E. PHEENEY. 1980. Peat fabric and structure. *Canadian Gotechnical Journals* **17:** 416-435.

MICHELL, J.K. 1993. *Fundamentals of Soil Behavior.* J. Wiley & Sons Inc.

MIYAKAWA, J. 1960. Soils engineering research on peats alluvia. Reports 1-3. *Hokkaido Development Bureau Bulletin* **20**. Civil Engineering Research Institute.

SKEMPTON, A.W. and D.J. PETLEY. 1970. Ignition loss and other properties of peats and clays from Avonmouth, King's Lynn & Cranberry Moss. *Geotechniques* **20(4):** 343-356.

TRESIDDER, J. O. 1966. An overview of existing methods of road constructions over peat. Road Research Technical Paper No. 40.

YOGESWARAN, M. 1995. Geological considerations in the development of Kuching area dialogue session. Geological and Geotechnical Considerations in Civil Works, Geological Survey of Malaysia. Kuala Lumpur.

Pertanika J. Sci. & Technol. **14(1 & 2)**: 75 - 80 (2006)
ISSN: 0128-7680

Chemical Constituents of Leaves and Barks of *Melicope hookeri* T.G. Hartley

[a]Nor Azah Mohamad Ali, [a*]Mawardi Rahmani, [a]Khozirah Shaari, [b]Hazar B.M. Ismail, [a]Mohd Aspollah Sukari, [c]Abdul Manaf Ali & [d]Julius Kulip

[a]Department of Chemistry, Universiti Putra Malaysia, 43400 UPM, Serdang, Selangor, Malaysia
[b]Centre for Foundation Study in Science, University Malaya, Kuala Lumpur, Malaysia
[c]Department of Biotechnology, Universiti Putra Malaysia, 43400 UPM, Serdang, Selangor, Malaysia
[d]Forest Department, PO Box No. 68, 90009 Sandakan, Sabah, Malaysia

Received: 9 March 2005

ABSTRAK

Kajian fitokimia terhadap daun dan kulit batang *Melicope hookeri* T.G. Hartley (Rutaceae) telah berjaya memencilkan dan mengenali tiga flavonoid, ayanin, ombium dan kumatakenin; dua koumarin, umbelliferone dan scopoletin; dan sitosterol. Struktur sebatian ini telah ditentukan dengan kajian mendalam menggunakan kaedah spektroskopi.

ABSTRACT

Phytochemical investigation on the leaves and bark of *Melicope hookeri* T.G. Hartley (Rutaceae) has resulted in the isolation and identification of three flavonoids, ayanin, ombuin and kumatakenin, two coumarins, umbelliferone and scopoletin and β-sitosterol. The structures of these compounds were determined by detailed spectroscopic methods.

Keywords: *Melicope hookeri*, ayanin, ombium, kumatakenin, umbelliferone scopoletin

INTRODUCTION

The genus *Melicope* is usually a shrub or small tree of the family Rutaceae. The plants are widely distributed throughout South East Asia right up to India, Madagascar, Polynesia and Northern Australia. Some members of the genus are traditionally used for the treatment of various ailments such as treatment of cold, rheumatism and spleen inflammation (Jones 1995). Many classes of chemical constituents have been reported to occur in these plants such as alkaloids, flavonoids, lignans, phloroglucinols, benzopyrans, coumarins and essential oils (Fauvel *et al.* 1981; Jong and Wu 1989; Kamperdick *et al.* 1997; Latip *et al.* 1999; Chan *et al.* 1989; Simonsen *et al.* 2002). In this work we wish

* Corresponding author:
E-mail: *mawardi@fsas.upm.edu.my*

to report the isolation of three flavonoids, two coumarins and β-sitosterol from the leaves and bark extracts of *Melicope* cf *hookeri* collected from Sandakan, Sabah.

RESULTS AND DISCUSSION

Ayanin (1) was obtained as yellowish needle-shaped crystals, m.p. 173-174°C with the typical UV absorptions of a flavonone skeleton at 356, 255 and 208 nm. The IR spectrum gave a strong and broad absorption at 3423 cm^{-1} which indicated the presence of hydroxyl group and another strong absorption at 1657 cm^{-1} for a carbonyl group. The mass spectrum gave a molecular ion peak at m/e 344 which corresponds to the molecular formula $C_{18}H_{16}O_7$. The aromatic region of the ^{1}H-NMR indicated the presence of five protons in which two occurred as mutually *meta*-coupled doublets at δ 6.33 and 6.69 (J = 1.5 Hz) assigned to H-6 and H-8 protons, respectively. The other three aromatic protons exhibited an ABX system with the appearance of a doublet of doublet at δ 7.71 (J = 8.0 Hz, 1.3 Hz) and two doublets at δ 7.67 (J = 1.3 Hz) and 7.14 (J = 8.0 Hz) due to protons H-6', H-2' and H-5', respectively. The spectrum also indicated the presence of three methoxyl groups with the occurrence of three proton singlets at δ 3.90, 3.95 and 3.97. A very low field broad singlet at δ 12.74 clearly indicated the presence of a chelated hydroxyl group and another hydroxyl group was also observed at δ 8.27 as a broad singlet. The ^{13}C-NMR spectrum indicated the presence of 18 carbon atoms. This further supported the molecular formula suggested of which three occurred as methoxyl groups, five as methine and nine as quarternary carbon atoms. The connectivity between carbons and the directly attached protons were shown by the HSQC spectrum. These spectral data together with the HMBC spectra and comparison with literature values, the compound was unambiguously elucidated as 3',5-dihydoxy-3',4',7-trimethoxyflavone or commonly called ayanin (1) (Wang *et al.* 1989).

Ombuin (2) was also isolated as white solid, m.p. 231-232°C with the typical UV absorptions at 368, 255 and 208 nm due to the flavonone skeleton. The IR spectrum absorptions are very similar to the above compound. The mass spectrum gave a molecular ion peak at m/e 330 which corresponds to the molecular formula $C_{17}H_{15}O_7$. The aromatic region of the ^{1}H-NMR showed a similar pattern of substitution as in ayanin (1) but differ in their chemical shifts and coupling constants. The spectrum revealed the presence of two methoxyl groups (δ 4.02 and 3.90) and three phenolic protons one of which was chelated occurring at δ 11.73. The ^{13}C-NMR spectrum further supported the presence of 17 carbon atoms with the occurrence of two methoxyl, five methine and ten quarternary carbons. The positions of the hydroxyl and methoxyl groups were established by heteronuclear correlations observed in the HSQC and HMBC spectra. Comparison of these spectral data with literature values indicated the compound is identical to ombuin (2), previously isolated from *Cassia laevigata* (Singh *et al.* 1980).

The third flavonoid, kumatakenin (3), was also isolated as yellowish needle-shaped crystals, m.p 248-249°C with similar UV spectrum absorptions at 347, 257 and 208 nm^{-1} as the above compound. The IR spectrum also revealed the presence of a highly chelated hydroxyl group with a strong and broad band at 3421 cm^{-1} and carbonyl absorption at 1663 cm^{-1}. The ^{1}H-NMR spectrum showed the presence of two methoxyl groups at δ 3.78 and 3.87. It also exhibited two *meta* coupled doublets at δ 6.33 and 6.49 with a coupling constant value of 2.0 Hz. The other aromatic protons occurred as an AA'BB' system giving the typical pair of doublets at δ 6.93 and 7.98 each with a coupling constant value of 8.0 Hz assigned to protons at H-2'/H-6' and H-3'/H-5', respectively. Hence, the compound was elucidated as 5,4'-dihydroxy-3,7-dimethoxyflavone or kumatakenin (3), previously isolated from *Heliotropium chenopodiaceum* var. *chenopodiaceum* (Urzua *et al.* 1998).

The two simple coumarins, unbelliferone (4) and scopoletin (5), were isolated from the ethyl acetate bark extract as white needles with m.p. 244-246°C and 204-206°C, respectively. The UV spectra of the two compounds gave similar absorptions at 324 and 205 nm, typical of coumarin nucleus. The mass spectrum of scopoletin showed a molecular ion peak m/e at 192, 30 mass unit higher than for umbelliferone due to the presence of a methoxyl group. The two compounds were previously isolated from *Peucedanum praeruptorum* (Kong *et al.* 1996).

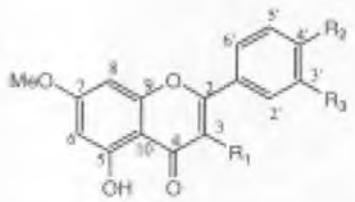

(1). R_1 = OMe, R_2 = OMe, R_3 = OH
(2). R_1 = OH, R_2 = OMe, R_3 = OH
(3). R_1 = OMe, R_2 = OH, R_3 = H

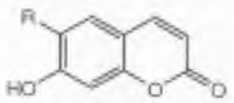

(4). R = H
(5). R = OMe

EXPERIMENTAL

General Experimental Procedures

Melting points were measured on a Kofler hot stage apparatus and are uncorrected. The IR spectra were recorded using KBr discs on Perkin Elmer FTIR spectrophotometer model 1275X. The UV spectrum was recorded on a Shimadzu UV 160A spectrophotometer in MeOH. The ^{1}H- and ^{13}C-NMR spectra were obtained on a Varian 500 MHz or JOEL FTNMR 400 MHz spectrometer. Chemical shifts are shown in δ values (ppm) with tetramethylsilane as an internal standard.

Plant Material

The leaves and stem bark of *Melicope hookeri* T.G. Hartley were obtained from Sepilok, Sabah, Malaysia and a voucher specimen was deposited at the Forest Research Centre, Sepilok, Sabah (accession numbers FRCES 398).

Extraction and isolation

The ground dried leaves and stem bark were separately and sequentially extracted in soxhlet extractor with petroleum ether, ethyl acetate and methanol each for 16 hours. The extracts were concentrated under reduced pressure to give dark viscous semi-solids. The petroleum ether leaves extract (30 g) was subjected to VLC and eluted with solvent gradient of petroleum ether, EtOAc and MeOH to afford 6 major fractions. Fractions 4 and 6 were subjected to a series of silica gel CC to give β-sitosterol (34 mg) and ayanin (1) (28 mg). The EtOAc extract (25 g) was separated by VLC eluted with hexane and gradual increase in $CHCl_3$ and EtOAc to give 8 fractions. Fractions 4-6 were further purified by a series of CC to give another sample of ayanin (1) (20 mg), ombuin (2) (11 mg) and kumatakenin (3) (16 mg). Chromatographic separation of the MeOH extract also afforded the three above compounds. The EtOAc extract of the bark (10 g) was also subjected to VLC and eluted with mixtures of hexane and EtOAc of increasing polarity to give 30 fractions of 100 ml each. Further CC separation of fractions 22-26 gave umbelliferone (4) (23 mg), scopoletin (5) (18 mg) and another sample of ayanin (1) (25 mg).

Ayanin (1), Isolated as yellowish needles, m.p. 173-174°C; UV λ_{max}, MeOH (log ε) nm: 356 (0.6), 255 (0.76) and 208 (1.2); IR n_{max} (KBr) cm^{-1}: 3554, 3423, 1657, 1620, 1590, 1505, 1367, 1328, 1257, 1215, 1161, 1094; ^{1}H-NMR (500 MHz, CD_3COCD_3) δ: 12.74 (1H, *brs*, OH-5), 8.27 (1H, *brs*, OH-3'), 7.71 (1H, *dd*, 1.3 Hz, 8.0 Hz, H-6'), 7.67 (1H, *d*, 1.3 Hz, H-2'), 7.14 (1H, *d*, 8.0 Hz, H-5'), 6.69 (1H, *d*, 1.5 Hz, H-8), 6.33 (1H, *d*, 1.5 Hz, H-6), 3.97 (OMe-4'), 3.95 (OMe-7), 3.90 (OMe-3); ^{13}C-NMR (125 MHz, CD_3COCD_3) *ppm*: 178.9 (C-4), 165.0 (C-7), 162.1 (C-9), 157.1 (C-5), 156.2 (C-3'), 150.4 (C-4'), 146.8 (C-2), 139.0 (C-3), 123.4 (C-1'), 121.1 (C-6'), 115.2 (C-2'), 111.5 (C-5'), 105.9 (C-10), 97.9 (C-6), 92.2 (C-8), 59.6 (C-3), 55.8 (C-7), 55.6 (C-4'); MS m/e (%): 344 (M^+, 100), 330 (12.5), 301 (32.9), 258 (10.3), 217 (13.6), 158 (22.9), 135 14.9), 120 (8.2), 69 (12.3).

Ombuin (2). Obtained as a white solid, m.p. 231-232°C; UV λ_{max}, MeOH (log ε) nm: 368 (0.85), 255 (0.96), 208 (1.30); IR ν_{max} (KBr) cm^{-1}: 3878, 3251, 3011, 2949, 1842, 1664, 1601, 1586, 1555, 1499, 1460, 1410, 1376, 1228 1098; ^{1}H-NMR (500 MHz, $CDCl_3$) *δ*: 11.73 (1H, *brs*, OH-5), 7.85 (1H, *d*, 8.5 Hz, H-5'), 7.81 (1H, *brs*, H-2'), 7.00 (1H, *d*, 8.5 Hz, H-6'), 6.62 (1H, *brs*, OH-3), 6.52 (1H, *brs*, H-8), 6.40 (1H, *brs*, H-6), 5.72 (1H, *brs*, OH-3'), 4.02 (3H, *s*, OMe-4'), 3.90 (3H, *s*, OMe-7); ^{13}C-NMR (125 MHz, $CDCl_3$) *ppm*: 176.6 (C-4), 166.2 (C-7), 161.7 (C-5), 156.6 (C-9), 156.0 (C-3'), 148.9 (C-4'), 146.6 (C-2), 137.8 (C-3), 121.2 (C-6'), 113.8 (C-2'), 110.7 (C-5'), 102.8 (C-10), 98.2 (C-6), 92.4 (C-8), 94.6 (C-1'), 56.3 (OMe-4'), 56.1 (OMe-7); MS m/e (%): 330 (M^+, 100), 315 (30), 301 (14), 287 (13), 259 (10), 231 (5), 151 (10), 149 (18), 135 (16).

Kumatakenin (3). Isolated as yellowish needles, m.p 248-249°C: UV λ_{max}, MeOH (log ε) nm: 347 (0.8), 257 (0.9), 208 (1.3); IR ν_{max} (KBr) cm^{-1}: 3421, 3257, 1663, 1601, 1499, 1459, 1432, 1376, 1347, 1286, 1228, 1139, 1098; ^{1}H-NMR (500 MHz, CD_3COCD_3) δ: 12.64 (1H, *s*, OH-4), 7.98 (2H, *d*, 8.0 Hz, H-3'/H-5'), 6.93 (2H, *d*, 8.0 Hz, H-2'/H-6'), 6.49 (1H, *d*, 2.0 Hz, H-8), 6.33 (1H, *d*, 2.0 Hz, H-6), 3.87 (3H, *s*, OMe-7), 3.78 (3H, *s*, OMe-3); ^{13}C-NMR (125 MHz, CD_3COCD_3) *ppm*: 179.0 (C-4), 165.8 (C-7), 161.5 (C-9), 159.2 (C-2), 157.5 (C-5), 157.1 (C-4'), 138.7 (C-3), 130.5 (C-3'/C-5'), 121.5 (C-1'), 115.8 (C-2'/C-6'), 106.0 (C-10), 98.1 (C-6) 92.4 (C-8), 61.3 (OMe-3), 55.7 (OMe-7'); MS m/e (%): 314 (M^+, 100), 295 (23), 271 (40), 167 (15), 143 (29), 131 (10), 121 (36).

Umbelliferone (4). Isolated as white needles, m.p. 244-246°C; UV λ_{max} MeOH (log ε) nm: 324 (0.71), 205 (0.97); IR ν_{max} (KBr) cm^{-1}: 3649, 3443, 3346, 3182, 1893, 1683, 1606, 1565, 1510, 1464, 1319, 1133; ^{1}H-NMR (400 MHz, $CDCl_3$) δ: 7.88 (1H, *d*, 8.5 Hz, H-4), 7.52 (1H, *d*, 8.5 Hz, H-5), 6.87 (1H, *dd*, 1.5 Hz, 8.4 Hz, H-6), 6.77 (1H, *d*, 1.5 Hz, H-8), 6.18 (1H, *d*, 8.5 Hz, H-3); ^{13}C-NMR (100 MHz, $CDCl_3$) δ: 161.1 (C-7), 160.6 (C-2), 156.5 (C-9), 144.2 (C-4), 129.9 (C-5), 113.3 (C-6), 112.3 (C-10), 102.8 (C-8); MS m/e (%): 162 (M^+, 91), 134 (100), 105 (42), 78 (57), 63 (24).

Scopoletin (5). Isolated as white needles, m.p. 204-206°C; ^{1}H-NMR (500 MHz, CD_3COCD_3) δ: 8.03 (1H, *s*, OH-7), 7.86 (1H, *d*, 9.5 Hz, H-4), 7.22 (1H, *s*, H-5), 6.82 (1H, *s*, H-8), 6.19 (1H, *d*, 9.5 Hz, H-3), 3.93 (3H, *s*, OMe-6); MS m/e (%): 192 (M^+, 100), 177 (48), 164 (38), 149 (56), 121 (27).

ACKNOWLEDGEMENTS

We wish to thanks the Malaysian government for financial support in the form of IRPA grant and Universiti Putra Malaysia for the facilities.

REFERENCES

Chan, J.A., E.A. Shultis, S.A. Carr, C.W. DeBrosse, D.S. Eggleston, T.A. Francis, L.J. Hyland, W.P. Johnson, L.B. Killmer, D.B. Staiger and J.W. Westley. 1989. Novel phloroglucinols from the plant *Melicope sessiflora* (Rutaceae). *J. Organic Chemistry* **54**: 2098-2103.

Fauvel, M.T., J. Gleye, C. Moulis, F. Blasco and E. Stanislas. 1981. Alkaloids and flavonoids of *Melicope indica*. *Phytochemistry* **20:** 2059-2060.

Jones, D.T. 1995. Rutaceae in tree flora of Sabah and Sarawak. In *FRIM, FD Sabah and FD Sarawak*, ed. E. Soepadmo and K.M. Wong, **1**: 351-419. Kuala Lumpur: Ampang Press.

Jong, T.T. and T.S. Wu. 1989. Highly oxygenated flavonoids from *Melicope triphylla*. *Phytochemistry* **28:** 245-246.

Kamperdick, C., N. H. Van, T.V. Sung and G. Adam. 1997. Benzopyrans from *Melicope ptelefolia*. *Phytochemistry* **45:** 1049-1056.

Kong, L.Y., Y. Li, Z.D. Min, X. Li and T.R. Zhu. 1996. Coumarins from *Peucedanum praeruptorum*. *Phytochemistry* **41:** 1423-1426.

LATIP, J., T. G. HARTLEY and P. G. WATERMAN. 1999. Lignans and coumarins metabolites from *Melicope hayesii*. *Phytochemistry* **51:** 107-110.

SIMONSEN, H. T., M. D. LARSEN, M. W. NIELSEN, A. ANDERSEN, C. E. OLSEN, D. STRASBERG, U. W. SMITT and J. W. JAROSZEWSKI. 2002. Methylenedioxy- and methoxy flavones from *Melicope cordeana* syn. *Evodia simplex* **60:** 817-820.

SINGH, J., A. R. TIWARI and R. D. TIWARI. 1980. Anthraquinones and flavonoids of *Cassia laevigata*. *Phytochemistry* **19:** 1253-1254.

URZUA, A., B. MODAK, L. VILLAROEL, R. TORRES and L. ANDRADE. 1998. Comparative falvonoids composition exudates from *Heliotropium chenopodium* var. *chenopodiaceum* and *H. chenopodiaceum* var. *ericoideum*. *Biochemical Systematics and Ecology* **26:** 127-130.

VASCONSELOS, J. M. J., A. M. S. SILVA and J. A. S. CAVLEIRO. 1998. Chromones and flananones from Artemisia campestris subsp. maritima. *Phytochemistry* **49:** 1421-1424.

WANG, Y., M. HAMBURGER, J. GUEHO and K. HOSTETTMANN. 1989. Antimicrobial flavonoids from *Psiadia trinervia* and their methylated and acetylated derivatives. *Phytochemistry* **38:** 2323-2327.

Pertanika Journal of Science & Technology

Subject Index for Vol. 14 Nos. 1 & 2 2006

Pertanika Journal of Science & Technology

Author Index for Vol. 14 Nos. 1 & 2 2006

ACKNOWLEDGEMENTS

The Editorial Board acknowledges the assistance of the following reviewers in the preparation of Volume 14, Numbers 1 & 2 of this journal

Assoc. Prof. Dr. Abd Rahman Ramli
Prof. Dr. Abdul Razak Daud
Dr. Anton Abdulbasah Kamil
Mr. Azlan A. Aziz
Assoc. Prof. Dr. Gwendoline Ee Cheng Lian
Prof. Dr. Ibrahim Jantan
Dr. Michael Khoo Boon Chong
Assoc. Prof. Dr. Mohamad Pauzi Zakaria
Prof. Dr. Mohd Maarof H.A. Moksin
Dr. Puziah Abd Latif
Assoc. Prof. Dr. Ramli Abu Hassan
Assoc. Prof. Dr. Saadah Abdul Rahman
Mr. Shukri Mail
Assoc. Prof. Dr. Zainal Abidin Talib